© 2017. Published by The Company of Biologists Ltd | Journal of Cell Science (2017) 130, 1662-1674 doi:10.1242/jcs.200758

RESEARCH ARTICLE

Intraflagellar transport protein IFT52 recruits IFT46 to the basal body and flagella

Bo Lv[1,2], Lei Wan[1], Michael Taschner[*,3], Xi Cheng[1,2], Esben Lorentzen[*,3] and Kaiyao Huang[1,‡]

ABSTRACT

Cilia are microtubule-based organelles and perform motile, sensing and signaling functions. The assembly and maintenance of cilia depend on intraflagellar transport (IFT). Besides ciliary localization, most IFT proteins accumulate at basal bodies. However, little is known about the molecular mechanism of basal body targeting of IFT proteins. We first identified the possible basal body-targeting sequence in IFT46 by expressing IFT46 truncation constructs in an *ift46-1* mutant. The C-terminal sequence between residues 246–321, termed BBTS3, was sufficient to target YFP to basal bodies in the *ift46-1* strain. Interestingly, BBTS3 is also responsible for the ciliary targeting of IFT46. BBTS3::YFP moves bidirectionally in flagella and interacts with other IFT complex B (IFT-B) proteins. Using IFT and motor mutants, we show that the basal body localization of IFT46 depends on IFT52, but not on IFT81, IFT88, IFT122, FLA10 or DHC1b. IFT52 interacts with IFT46 through residues L285 and L286 of IFT46 and recruits it to basal bodies. Ectopic expression of the C-terminal domain of IFT52 in the nucleus resulted in accumulation of IFT46 in nuclei. These data suggest that IFT52 and IFT46 can preassemble as a complex in the cytoplasm, which is then targeted to basal bodies.

KEY WORDS: *Chlamydomonas*, Intraflagellar transport, Basal body, Targeting sequence

INTRODUCTION

Eukaryotic cells evolved different types of organelles that carry out specialized functions. One of them is the cilium, also known as flagellum, which is found on most eukaryotic cells. Cilia are hair-like microtubule-based organelles that protrude from the cell surface and are composed of the axoneme, ciliary matrix and ciliary membrane (Mizuno et al., 2012; Satir and Christensen, 2007). Cilia primarily play two vital roles (Satir and Christensen, 2007). One is to function as a cellular motor to move either the cell itself or surrounding liquids/particles. The other function of cilia is to serve as a hub for cellular signaling (Ishikawa and Marshall, 2011; Mourão et al., 2016; Singla and Reiter, 2006; Wood and Rosenbaum, 2015). Defects in ciliary structures and functions in humans lead to diseases commonly referred to as 'ciliopathies', such as polycystic kidney disease, blindness, heterotaxy, Bardet–Biedl syndrome and skeletal abnormalities (Fliegauf et al., 2007; Gerdes et al., 2009; Hildebrandt et al., 2011; Hildebrandt and Zhou, 2007).

The formation and maintenance of cilia, as well as ciliary signaling, depend on intraflagellar transport (IFT) (Ishikawa and Marshall, 2011; Mourão et al., 2016; Pedersen and Rosenbaum, 2008; Scholey, 2003), a bidirectional movement of granular particles between the outer doublet microtubules and the flagellar membrane along the cilium (Kozminski et al., 1993). The anterograde (base to tip) movement of IFT particles is powered by kinesin-2 (Kozminski et al., 1995; Miller et al., 2005; Ou et al., 2005; Pan et al., 2006; Snow et al., 2004; Walther et al., 1994), while cytoplasmic dynein 2 or dynein 1b drives retrograde IFT (tip to base) (Hou et al., 2004; Pazour et al., 1999). More than 22 IFT proteins form at least three biochemically distinct complexes, namely IFT-A, IFT-B1 and IFT-B2 (Taschner and Lorentzen, 2016; Taschner et al., 2016). Since cilia lack the machinery for protein synthesis, proteins – including structural components and signaling molecules – are synthesized in the cell body, and some are delivered into cilia via IFT. IFT and cargos may assemble into periodic IFT trains (Pigino et al., 2009; Stepanek and Pigino, 2016; Vannuccini et al., 2016). Anterograde IFT occurs over a distance of about 233 nm and moves along B-microtubules. Retrograde IFT occurs over a distance of about 209 nm and moves along A-microtubules (Pigino et al., 2009; Stepanek and Pigino, 2016). In addition, IFT proteins also function in other cellular processes, including vesicle exocytosis, cell division and the formation of immunological synapses and microtubule-based nanotubes (Baldari and Rosenbaum, 2010; Borovina and Ciruna, 2013; Griffiths et al., 2010; Inaba et al., 2015; Wood et al., 2012).

In addition to the dynamic movement of IFT in cilia, nearly all IFT and motor proteins are concentrated at the basal body. The IFT-B proteins and anterograde motor appear as a semi-circular tri-lobed arc, and the IFT-A proteins and retrograde motor appear as a semi-circular di-lobed arc (Brown et al., 2015; Deane et al., 2001). The two anterior lobes (pool) are colocalized (Brown et al., 2015). However, the mechanism of the basal body localization of IFT subunits, which is one of the key steps in the initiation of ciliogenesis, remains largely unknown. Since the the IFT proteins, such as IFT46, are localized in trans-Golgi network (TGN)-derived vesicles during flagellar regeneration, Woods et al. have suggested that IFT complexes may associate with the vesicle first, recruit the cargos, and then be targeted to the basal body (Wood and Rosenbaum, 2014). Many ciliary proteins, especially ciliary membrane proteins, contain ciliary-targeting sequences (CTSs) (Bhogaraju et al., 2013; Malicki and Avidor-Reiss, 2014). These CTSs mediate the basal body and ciliary localization of target proteins. However, CTSs are diverse, which suggests different transporting systems participate in these processes (Bhogaraju et al., 2013; Malicki and Avidor-Reiss, 2014). Well-characterized cases

[1]Key Laboratory of Algal Biology, Institute of Hydrobiology, Chinese Academy of Sciences, Wuhan, Hubei 430072, China. [2]University of Chinese Academy of Sciences, Beijing 100039, China. [3]Department of Structural Cell Biology, Max-Planck-Institute of Biochemistry, Martinsried D-82152, Germany.
*Present address: Department of Molecular Biology and Genetics, Aarhus University, Gustav Wieds Vej 10c, DK-8000, Aarhus C, Denmark.

[‡]Author for correspondence (huangky@ihb.ac.cn)

B.L., 0000-0002-3448-8986; L.W., 0000-0003-2064-9643; M.T., 0000-0002-3789-5077; X.C., 0000-0003-2117-4707; E.L., 0000-0001-6493-7220; K.H., 0000-0001-8669-1065

Received 22 December 2016; Accepted 14 March 2017

Journal of Cell Science

Journal of Cell Science (2017) 130, 1662-1674 doi:10.1242/jcs.200758

are motifs found in the third intracellular loop of different G-protein-coupled receptors (GPCRs), the Ax(S/A)xQ and RVxP motifs (where x indicates any amino acid), nuclear localization signal and SUMOylation (Bhogaraju et al., 2013; Dishinger et al., 2010; Malicki and Avidor-Reiss, 2014; McIntyre et al., 2015). Nonetheless, none of them has been found in IFT proteins.

Some factors such as BBS7, BBS8, C2cd3, CCDC41, OFD1, Rsg1 and TTBK2 affect the recruitment of certain IFT subunits to the basal body (Blacque et al., 2004; Brooks and Wallingford, 2013; Goetz et al., 2012; Joo et al., 2013; Ye et al., 2014), but their functions are unspecific (Toriyama et al., 2016). Recently, ciliogenesis and planar polarity effectors (CPLANEs), including Jbts17, Intu, Fuz, Wdpcp and Rsg1, have been shown to recruit peripheral IFT-A proteins to basal bodies (Brooks and Wallingford, 2012; Toriyama et al., 2016). This finding represents a real breakthrough, although the CPLANE proteins may be required for the stability and assembly of peripheral IFT-A complexes rather than direct basal body recruitment (Toriyama et al., 2016).

In this paper, we explored the molecular mechanism of the basal body localization of IFT46 and found that the C-terminus of IFT46 mediates its basal body localization. The targeting sequence can assemble into the IFT complex, which moves along the flagellum. Biochemical and genetic studies showed that IFT52 binds and recruits IFT46 to basal bodies. These new findings suggest that IFT52 and IFT46 preassemble in the cytoplasm or the TGN but not in the basal body.

RESULTS

YFP-tagged IFT46 functions like the endogenous form and localizes at the basal body and flagella

To study the molecular mechanism of IFT accumulation at the basal body, we focused on one pivotal subunit of IFT-B1, IFT46, since both the null mutant (*ift46-1*) and a specific antibody are available (Hou et al., 2007). We firstly fused Citrine Yellow fluorescent protein (YFP) to the C-terminus of IFT46 with a linker peptide in between (Fig. 1A) (Griesbeck et al., 2001; Long and Huang, 2012). YFP-tagged IFT46 was then expressed in *ift46-1* (Hou et al., 2007). The null mutant has stumpy, paralyzed flagella and can transcribe the 5′ end of the *IFT46* gene (Hou et al., 2007). In theory, rescued strains will thus have full-length flagella and swim normally. Indeed, we identified 52 rescued strains among 132 transformants (Movies 1–3). The middle part and C-terminus of *IFT46* were only expressed in wild-type (WT) and the *ift46-1* strain expressing *IFT46::YFP* (*ift46-1 IFT46::YFP*). The YFP was only expressed in *ift46-1 IFT46::YFP* (Fig. 1B). *IFT46* was transcribed to equal extents in WT and in *ift46-1 IFT46::YFP* (Fig. 1C). Subsequently, four strains were chosen randomly for immunoblotting analysis. A 75 kDa protein was only detected in *ift46-1 IFT46::YFP*, not in WT (Fig. 1D), suggesting it is the fusion protein IFT46::YFP. The expression level of IFT46 in WT and of IFT46::YFP in rescued strains were nearly equal ($P>0.05$, Fig. 1D). These data demonstrate that the endogenous promoter of *IFT46* drives the expression of IFT46::YFP efficiently.

To evaluate the influence of the YFP tag on the function of IFT46, we compared flagella-related phenotypes of *ift46-1 IFT46::YFP* with WT. The average ciliary lengths and the percentages of ciliated cells of the rescued strains were akin to those of WT cells (Fig. S1A,B). The anterograde and retrograde transport velocities and frequencies of IFT46::YFP were similar to results published previously (Fig. S1C,D,E, Movie 4) (Brown et al., 2015). In summary, these data demonstrate that the 28 kDa YFP tag does not affect the motility and function of IFT46.

Due to the stumpy paralyzed flagella, the daughter cells of *ift46-1* are restricted in the mother cell wall (Movies 1–3) (Hou et al., 2007). When rescued, the cells grew flagella of normal length (Fig. 1E; Fig. S1A). IFT46::YFP accumulated at basal bodies and localized in a dotted pattern along the flagella (Fig. 1E). We also expressed only YFP in *ift46-1* as a negative control. Free YFP accumulated around the nuclei in *ift46-1 YFP* (Fig. 1E). These data confirmed that the basal body localization of IFT46::YFP is specific. Moreover, the punctate pattern of IFT46::YFP along the flagella was more obvious when examined by total internal reflection fluorescence microscopy (TIRFM) (Fig. 1F). IFT46::YFP also moved along the axoneme bidirectionally, just as other IFT subunits did (Movie 4). Collectively, these data suggest that the rescued strains can be used to study the molecular mechanism of IFT accumulation at basal bodies.

BBTS3 targets IFT46 to the basal body

IFT46 is mainly composed of α helices and random coils (Fig. S2A). The N-terminus and glycine-rich tail of IFT46 are predicted to be intrinsically unstructured and disordered (Fig. S2B). To identify the targeting sequence in IFT46 responsible for its basal body localization, we generated and expressed a series of truncated IFT46 constructs fused with YFP in *ift46-1* according to the secondary structure of IFT46 and potential domain boundaries (Buchan et al., 2013; Jones, 1999) (Fig. 2A,C; Fig. S2). These truncated IFT46 constructs were named IFT46-N1, IFT46ΔN1, IFT46-N, IFT46-C, IFT46ΔC1 and IFT46-C1, respectively (Fig. 2A). Since none of these truncated forms can fully or partially rescue the null mutant, positive transformants were screened and identified using immunoblotting with an antibody against GFP (Fig. 2C). All fusion proteins were expressed with predicted molecular weights (Fig. 2C). For example, the predicted molecular weight of IFT46-N::YFP is about 46.3 kDa, and it migrated at 50 kDa on SDS-PAGE (Fig. 2C). Then, the localization of truncated IFT46 in cell bodies was determined by confocal imaging. The fusion proteins IFT46-N1::YFP, IFT46-N::YFP and IFT46ΔC1::YFP were evenly distributed across cell bodies and did not accumulate at the basal body (Fig. 2E). By contrast, the fusion proteins IFT46ΔN1::YFP, IFT46-C::YFP and IFT46-C1::YFP localized at basal bodies (Fig. 2E). Since all these fusion proteins that localized at the basal body contain the C1 domain, this suggests that the C1 domain is necessary and sufficient for basal body targeting of IFT46. In other words, IFT46-C1 may contain the basal body targeting sequence of IFT46.

As most known ciliary targeting sequences are shorter than IFT46-C1 (99 amino acids) (Berbari et al., 2008; Bhogaraju et al., 2013; Dishinger et al., 2010; Hurd et al., 2011; Malicki and Avidor-Reiss, 2014; McIntyre et al., 2015; Santos and Reiter, 2014), we further truncated IFT46-C1 and expressed the resulting constructs in *ift46-1* (Fig. 2B,D). These constructs were named as BBTS1 to BBTS6, sequentially (Fig. 2B). Positive transformants expressing the fusion proteins were identified by immunoblotting. These fusion proteins were expressed to nearly equal extents, running in the gel at the predicted molecular weights, in the null mutant *ift46-1* (Fig. 2D). We found that only BBTS3::YFP localized at the basal body (Fig. 2F). Therefore, BBTS3 is the shortest basal body localization sequence (76 amino acids) of IFT46 that we were able to identify.

BBTS3 targets IFT46 to cilia and moves along the ciliary axoneme

We have demonstrated above that the IFT46-C1 and BBTS3 are necessary and sufficient for the basal body targeting of IFT46. The

Journal of Cell Science (2017) 130, 1662-1674 doi:10.1242/jcs.200758

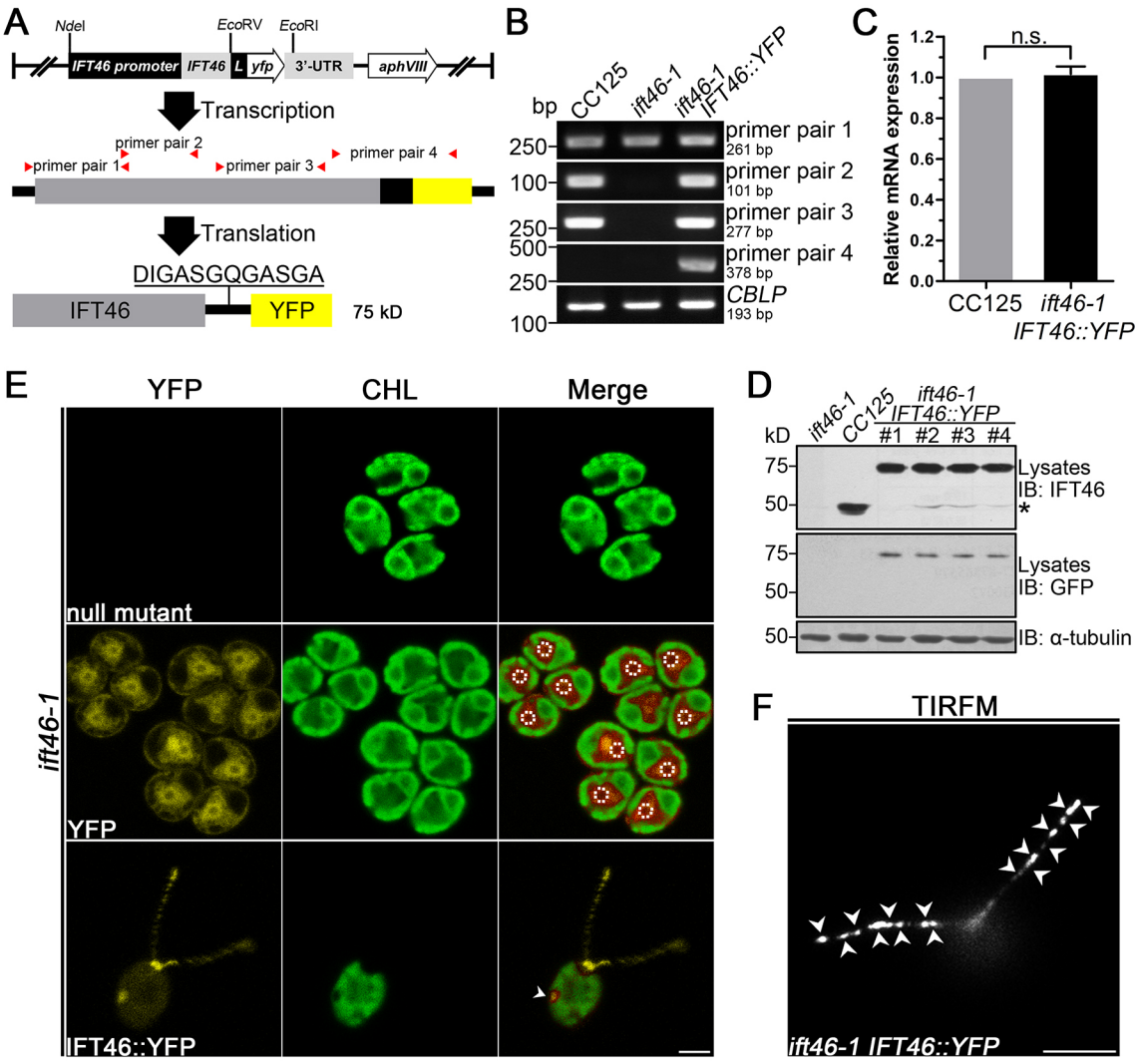

Fig. 1. YFP-tagged IFT46 localizes at the basal body and flagella. (A) Schematic diagram of the construct used to rescue *ift46-1*. Its predicted transcript and corresponding protein in *C. reinhardtii* are also shown below. L, protein linker sequence. Red triangles represent primer pairs used to detect mRNA of *IFT46* and *IFT46::YFP*. (B) Reverse-transcription PCR with cDNA templates from WT, *ift46-1* and rescued cells *ift46-1 IFT46::YFP* using primers designed to amplify transcripts from the 5′ (primer pair 1), middle (primer pair 2) and 3′ (primer pair 3) regions of the *IFT46* gene and *YFP* gene (primer pair 4). Expression of *CBLP* was used as the internal control. Primers are listed in Table S3. (C) Quantification of the expression level of *IFT46* in *ift46-1 IFT46::YFP* using real-time PCR (five samples for each group). Values were normalized to the expression level of *IFT46* in WT cells and expressed as mean±s.e.m. Statistical analysis was performed using two-tailed unpaired Student's *t*-test. n.s., not significant. (D) Western blot analysis of whole-cell lysates (5 µg protein per lane) of *ift46-1*, CC-125 and *ift46-1 IFT46::YFP* strains probed with antibodies raised against IFT46, GFP or α-tubulin. The asterisk indicates nonspecific bands. IB, immunoblot. (E) Live-cell imaging of non-transformed *ift46-1* cells and *ift46-1* expressing YFP or IFT46::YFP. White dashed circles mark the nucleus area. White arrowhead, eyespot; CHL, chlorophyll. Scale bar: 5 µm. (F) TIRFM imaging of the flagella of *ift46-1 IFT46::YFP*. White arrowheads mark IFT trains. Scale bar: 5 µm.

next question is whether they can also target IFT46 to cilia. To address this, the full-length and truncated IFT46 constructs were expressed in WT cells, which have normal flagella. Positive transformants expressing the fusion proteins were identified by immunoblotting with an antibody against GFP. All fusion proteins were expressed with the predicted molecular weights (Fig. 3A,B). The localization of the fusion proteins was determined using confocal microcopy. IFT46::YFP, IFT46ΔN1::YFP, IFT46-C::YFP and IFT46-C1::YFP localized predominantly in basal bodies (Fig. 3D) and flagella (Fig. 3C,D). In addition, these four proteins could be seen moving along the axoneme under live-cell imaging (Fig. 3F; Movies 5–8). However, IFT46-N1::YFP, IFT46-N::YFP and IFT46ΔC1::YFP did not accumulate at basal bodies (Fig. 3D). Interestingly, we could detect these proteins in flagella by western blotting analysis (Fig. 3C). Using TIRFM imaging, we also observed evenly weak and immobile fluorescence signals of YFP along the entire length of flagella (Fig. 3F), which is completely different to the dotted localization patterns seen with full-length IFT46::YFP, IFT46ΔN1::YFP, IFT46-C::YFP and IFT46-C1::YFP in flagella. As the molecular mass of these soluble proteins, such as IFT46-N1::YFP, IFT46-N::YFP and IFT46ΔC1::YFP, are all less than 100 kDa, it is reasonable to speculate that they enter cilia by diffusion through the transition zone (Breslow et al., 2013). These results not only confirmed the previous conclusion that IFT46-C1 can target IFT46 to basal bodies, but they also demonstrated that IFT46-C1 can target IFT46 to cilia.

As BBTS3 is the shortest basal body localization sequence of IFT46 we have identified so far, we questioned whether BBTS3 is also the ciliary localization sequence of IFT46. When the fusion construct was transformed into WT cells, positive clones could not

Journal of Cell Science (2017) 130, 1662-1674 doi:10.1242/jcs.200758

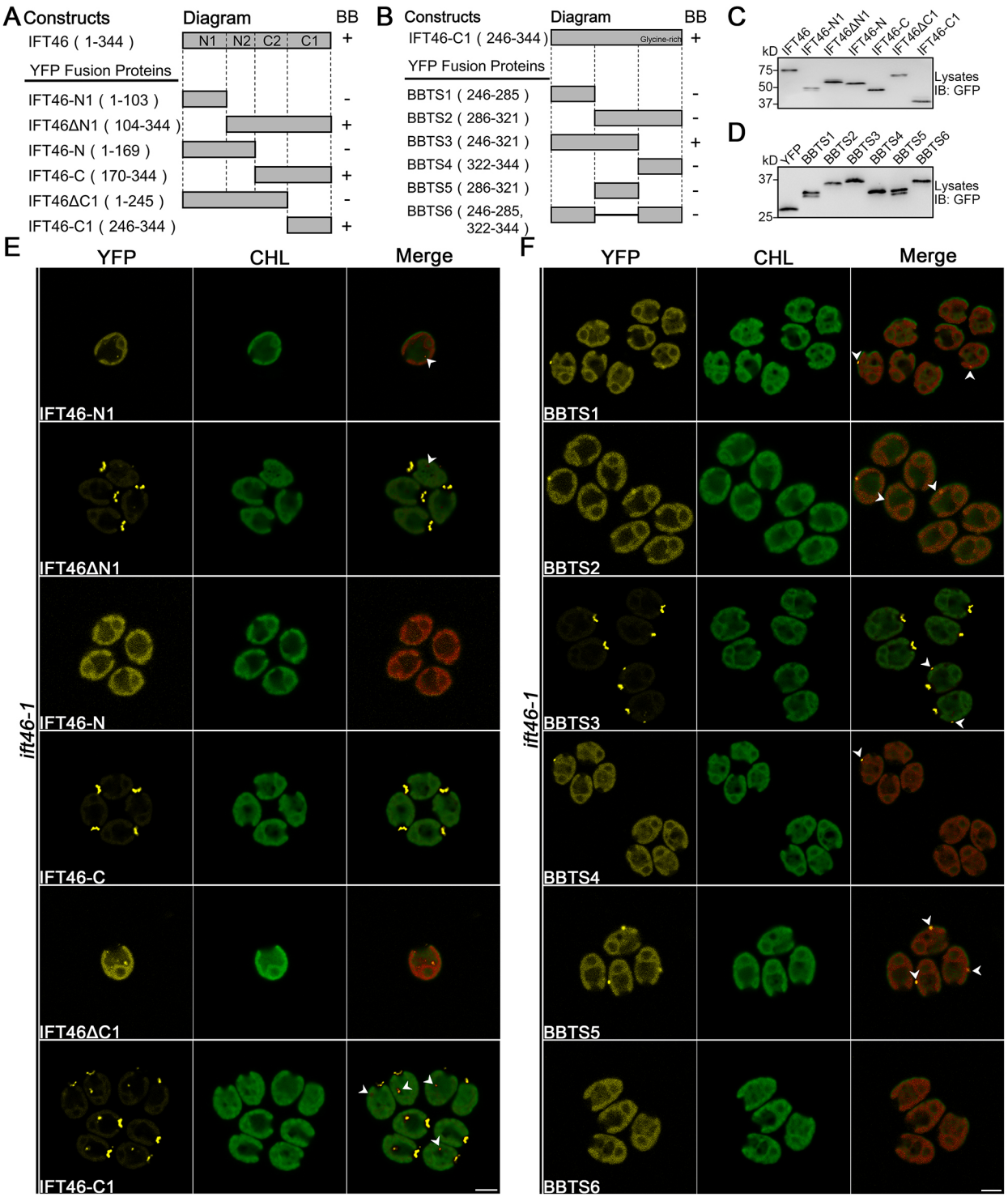

Fig. 2. IFT46-C1 and BBTS3 target IFT46 to the basal body. (A) Diagram of the full-length and the truncated IFT46 proteins produced in this study. YFPs are fused to the C-terminus of full-length and the truncated IFT46 proteins. (B) Diagram of the truncation constructs of IFT46-C1. (C,D) Immunoblots of whole-cell lysates (5 µg protein per lane) of *ift46-1* expressing the indicated proteins probed with an antibody against GFP. IB, immunoblot. (E) Confocal imaging of *ift46-1* expressing the indicated fusion proteins. White arrowheads, eyespots; CHL, chlorophyll. Scale bar: 5 µm. (F) Confocal images of *ift46-1* expressing the indicated fusion proteins. 'BB' in A and B represents the basal body localization results of the fusion proteins; +, yes; –, no. In E and F, arrowheads indicate eyespots. Scale bars: 5 µm.

be obtained in 200 transformants, as analyzed by immunoblotting. That may be caused by the low expression level or instability of BBTS3 in WT cells in the presence of full-length IFT46. As we were able to express BBTS3 in *ift46-1* (Fig. 2D), we then co-transformed *IFT46* and a selection marker pHyg3 into strain *ift46-1 BBTS3::YFP*, resulting in *ift46-1 BBTS3::YFP IFT46*, which is genetically comparable to CC-125 *BBTS3* (Fig. 3C). Confocal and TIRFM imaging revealed that BBTS3 also localized at flagella in a dotted pattern and moved along the axoneme (Fig. 3E,F; Movie 9). In summary, BBTS3 can also target IFT46 to cilia. Compared with

Journal of Cell Science

Journal of Cell Science (2017) 130, 1662-1674 doi:10.1242/jcs.200758

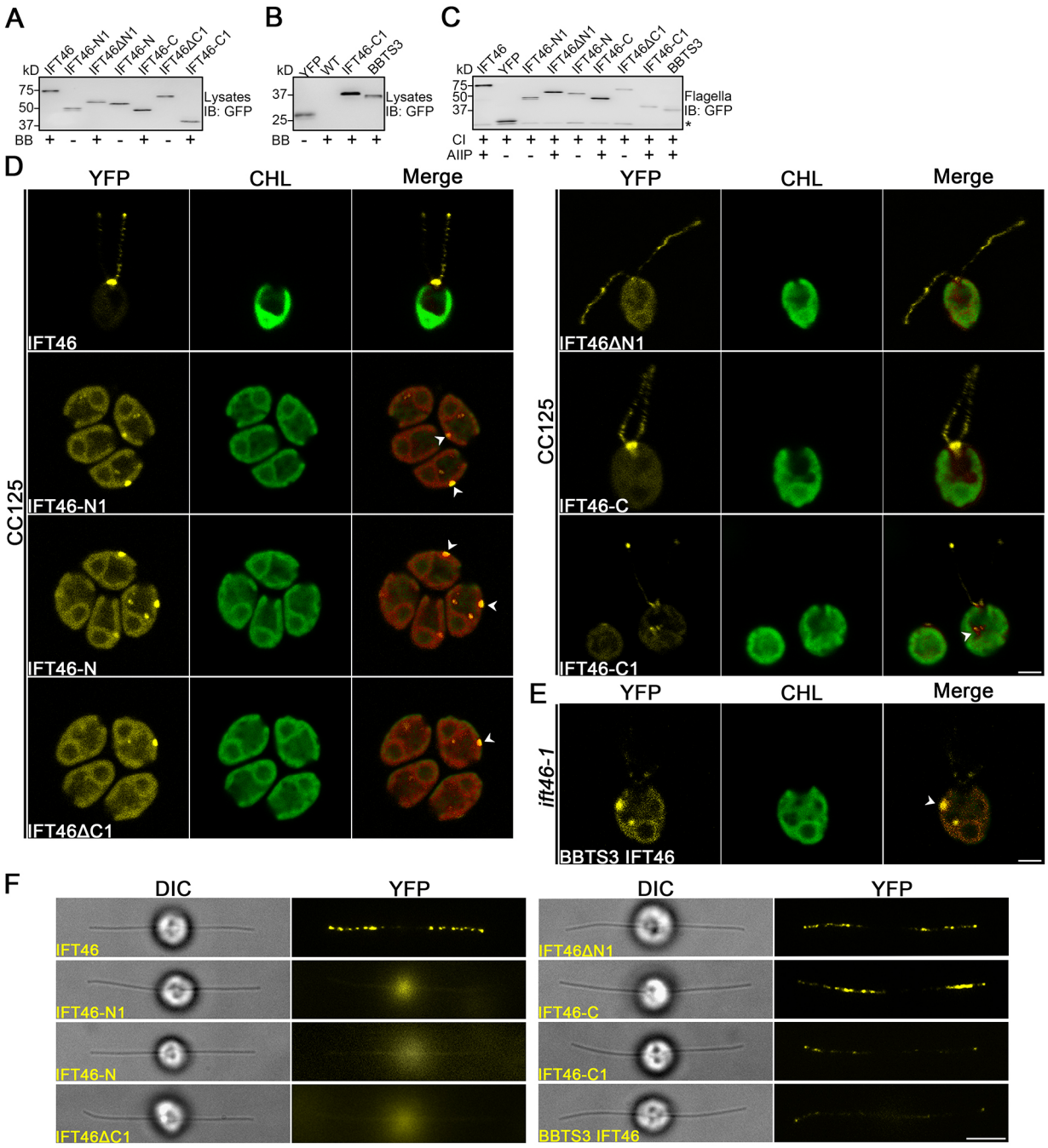

Fig. 3. IFT46-C1 and BBTS3 target IFT46 to cilia and move along axonemes. (A,B) Immunoblots of whole-cell lysates (5 µg protein per lane) of CC-125 expressing the indicated proteins probed with the antibody against GFP. +, protein localizes at the basal body (BB); –, protein does not localize at the BB. IB, immunoblot. (C) Immunoblot of flagellar membrane-plus-matrix fractions of CC-125 expressing the indicated proteins probed with the indicated antibodies. +, proteins localized in cilia (CI) or assembled in IFT particles (AIIP); –, no localization or assembly in IFT particles as indicated. IB, immunoblot. (D) Confocal imaging of CC-125 cells expressing the indicated fusion proteins. White arrowheads, eyespots; CHL, chlorophyll. Scale bar: 5 µm. (E) Confocal imaging of *ift46-1* expressing BBTS3::YFP and IFT46. White arrowheads, eyespots; CHL, chlorophyll. Scale bar: 5 µm. (F) TIRFM imaging of the flagella of the strains listed in D and E. Differential interference contrast (DIC) images are shown on the left. CHL, chlorophyll. Scale bar: 5 µm.

IFT46-C1, BBTS3 lacks the glycine-rich tail (Fig. 2B; Fig. S3), which may contribute to its stability. For this reason, IFT46-C1 was chosen for subsequent studies.

IFT46-C1 is assembled into the IFT machinery

IFT46-C1 and BBTS3 are able to move along the axoneme, and are likely to be incorporated into IFT-B complexes as part of IFT46. To prove this, we isolated and analyzed the flagellar membrane-plus-matrix fraction of the CC-125 strain expressing *IFT46-C1::YFP* and performed co-immunoprecipitation experiments. We found that IFT46-C1 forms a complex with IFT81, IFT72/74, and IFT52, just as full-length IFT46 does (Fig. 4A). Results of sucrose density gradient centrifugation also showed that IFT46-C1 forms a complex with IFT-B complex protein IFT81 (Fig. 4B). Overall, the data suggest that IFT46-C1 is assembled into the IFT machinery.

Journal of Cell Science (2017) 130, 1662-1674 doi:10.1242/jcs.200758

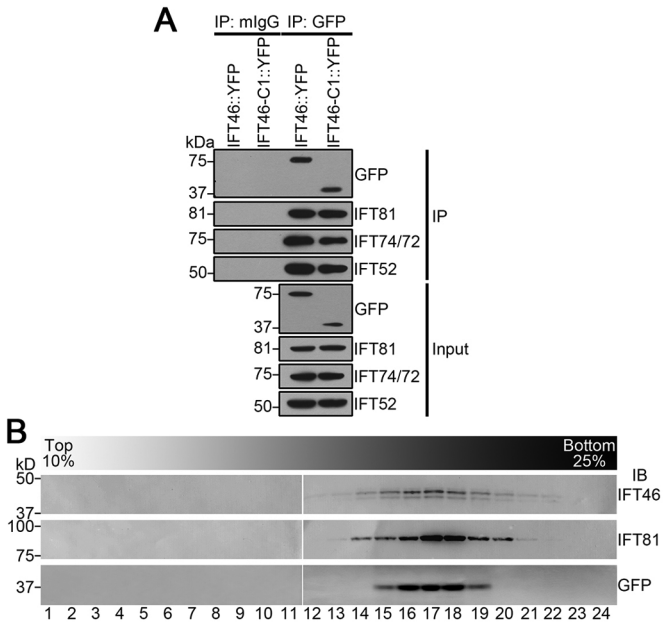

Fig. 4. IFT46-C1 is assembled into IFT machinery. (A) An antibody against GFP was used to immunoprecipitate YFP-tagged IFT46-C1 from the flagellar membrane-plus-matrix of *ift46-1 IFT46::YFP* and CC-125 *IFT46-C1::YFP*. Immunoblots of the precipitate were probed with antibodies against IFT81, IFT72/74 and IFT52. mIgG, mouse IgG; IP, immunoprecipitation. (B) Flagellar membrane-plus-matrix of CC-125 *IFT46-C1::YFP* was separated by sucrose density gradient centrifugation and analyzed by immunoblotting with antibodies against the indicated proteins. IFT46 migrates as doublet bands due to phosphorylation. IB, immunoblot. Numbers at the bottom indicate fractions.

The localization of IFT46 to the basal body region depends on IFT52, but not vice versa

As IFT46 interacts at least with ODA16, IFT88, IFT81, IFT74, IFT70 and IFT52 (Ahmed et al., 2008; Fan et al., 2010; Lucker et al., 2005, 2010; Taschner et al., 2011, 2014), we next determined whether the basal body localization of IFT46 is dependent on other IFT components. If so, this typical accumulation will be abolished in corresponding null mutants. Accordingly, we expressed full-length IFT46::YFP and IFT46-C1::YFP in *bld1*, *ift88*, *fla10-2* and *dhc1b* (Fig. 5A,B; Fig. S4A,B, D,E,G,H). These strains are null mutants of *IFT52*, *IFT88*, *FLA10* and *DHC1b*, respectively. Positive transformants expressing IFT46::YFP or IFT46-C1::YFP were screened using western blotting with an antibody against GFP (Fig. 5A,B). We also examined the subcellular localization of IFT46 in *ift81-2* and *ift122-1* strains using immunostaining (Fig. S4J,K). IFT46 and IFT46-C1 still localized at the basal body region in *ift88*, *fla10-2* or *dhc1b* (Fig. S4C,F,I). These results demonstrated that the basal body localization of IFT46 is independent of IFT88, FLA10 or DHC1b. In *ift81-2* or *ift122-1*, IFT46 colocalized with acetylated α-tubulin, which was predominantly located at the basal body and the stumpy flagella (Fig. S4J,K). This implies that the basal body localization of IFT46 is not disturbed. These data demonstrate that the basal body localization of IFT46 is independent of IFT81 or IFT122. Surprisingly, IFT46 or IFT46-C1 was not targeted to the basal body region in *bld1* (Fig. 5C). IFT52 is at the center of the IFT-B complex and makes several interactions with both IFT-B1 and IFT-B2 subunits (Lucker et al., 2005, 2010; Taschner et al., 2011, 2014, 2016; Taschner and Lorentzen, 2016). The failure of basal body localization of IFT46 or IFT46-C1 in *bld1* is unlikely to be caused by their decreased expression level as we used algal strains that highly expressed IFT46 or IFT46-C1 (Fig. 5A,B). In summary, the basal body localization of IFT46 depends upon IFT52.

Knock out of *IFT52* disrupts the basal body localization of IFT46. In theory, IFT46 will restore its basal body localization when *bld1* is rescued by IFT52. Under that scenario, we expressed IFT52::3HA (where 3HA denotes three hemagglutinin epitopes) in *bld1 IFT46::YFP* or *bld1 IFT46-C1::YFP* (Fig. 5D,E). Indeed, IFT46::YFP and IFT46-C1::YFP were targeted to the basal body region in *bld1 IFT46::YFP IFT52::3HA* and *bld1 IFT46-C1::YFP IFT52::3HA* (Fig. 5F). These results further demonstrate that the basal body localization of IFT46 relies on IFT52. However, there are two possibilities. One is that the dependence is mutual and IFT52 and IFT46 work together to complete basal body targeting. The other is that IFT52 works upstream of IFT46 and recruits IFT46 to basal bodies. To exclude one of these possibilities, we expressed IFT52::YFP in *ift46-1*. Positive transformants were screened using western blotting with an antibody against GFP (Fig. 5G). Live-cell imaging showed that IFT52 accumulated around the basal body region (Fig. 5H). This indicates that the basal body localization of IFT46 depends on IFT52, but not vice versa.

IFT52 binds to and recruits IFT46 to the basal body region

The direct interaction between IFT46 and IFT52 has been demonstrated previously *in vitro* (Fan et al., 2010; Lucker et al., 2005, 2010; Taschner et al., 2011, 2014). We showed above that IFT46 relies on IFT52 for its basal body localization *in vivo* (Fig. 5). It is reasonable to speculate that the protein–protein interaction between IFT46 and IFT52 may mediate basal body localization of IFT46. Indeed, co-immunoprecipitation using whole-cell lysates of *bld1 IFT46-C1::YFP IFT52::3HA* and an antibody against HA showed that IFT46 and IFT46-C1 were enriched in precipitates. Thus, IFT46 interacts with IFT52 through its C1 domain (Fig. 6A). To further test whether the interaction is necessary for the basal body localization of IFT46, we mutated two critical hydrophobic leucine residues (L285 and L286) to glutamic acid in IFT46-C1 (IFT46-C1$^{L285E/L286E}$; Fig. 6B; Fig. S3). These two sites are evolutionarily conserved (Fig. S3) and located in the binding interface between IFT52C and IFT46C in *C. reinhardtii* (Fig. 6C), as highlighted in the three-dimensional structure, modeled on the *Tetrahymena thermophile* IFT52C–IFT46C subcomplex crystal structure (Taschner et al., 2014). The L285E/L286E mutant of IFT46 no longer bound to the tagged C-terminal domain of IFT52 when co-expressed in *Escherichia coli*, even though it was expressed at the same level as the WT IFT46 protein (Fig. 6D). When expressed in *ift46-1*, the expression level of IFT46-C1$^{L285E/L286E}$ declined to 32% (on average) of that of the non-mutated form of IFT46-C1 (Fig. 6E,F). This is in accordance with the fact that IFT46$^{L285E/L286E}$ does not form a subcomplex with IFT52 *in vitro* (Fig. 6D). The decreased expression level may be in large part due to degradation of free IFT46-C1$^{L285E/L286E}$. As shown in Fig. 6G, mutation of residues 285 and 286 in IFT46-C1 abolished its basal body localization. Because IFT46-C1 still localized at basal bodies when it had a low expression level in the CC-125 line (Fig. 3D; data not shown), the loss of the basal body localization of IFT46-C1$^{L285E/L286E}$ cannot be ascribed to its low expression level. These results indicate that the interaction between IFT46-C1 and IFT52 is of vital importance for the basal body localization of IFT46. IFT52 binds to and recruits IFT46 to the basal body region.

Journal of Cell Science (2017) 130, 1662-1674 doi:10.1242/jcs.200758

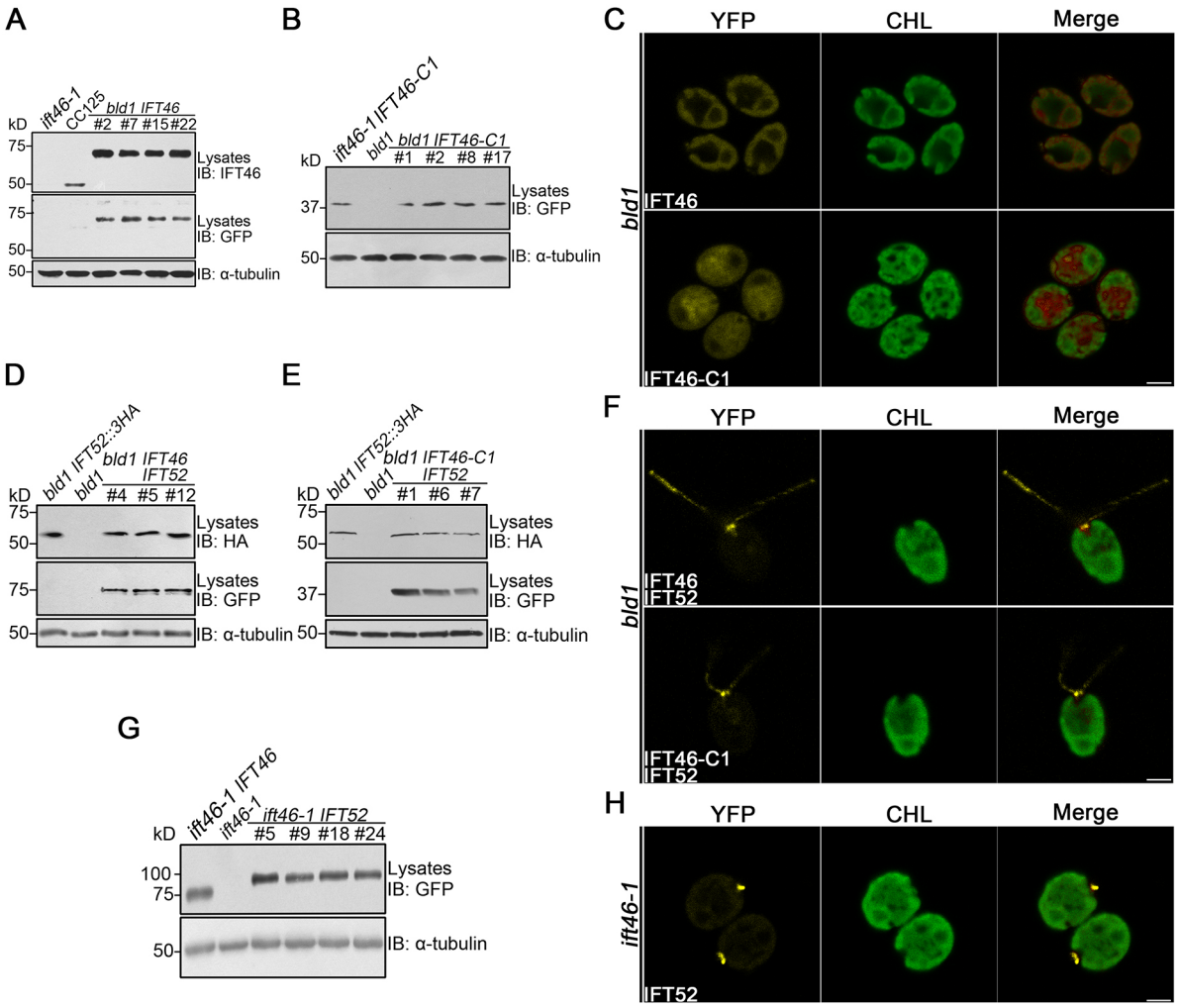

Fig. 5. The basal body localization of IFT46 depends on IFT52, but not vice versa. (A) Western blots of whole-cell lysates (5 µg protein per lane) of *bld1*, CC-125 and *bld1 IFT46::YFP* (*bld1 IFT46*) probed with antibodies against GFP and α-tubulin. IB, immunoblot. (B) Western blots of whole-cell lysates (5 µg protein per lane) of *ift46-1 IFT46-C1::YFP*, *bld1* and *bld1 IFT46-C1::YFP* (*bld1 IFT46-C1*) probed with the indicated antibodies. IB, immunoblot. (C) Confocal imaging of *bld1* expressing IFT46::YFP or IFT46-C1::YFP. CHL, chlorophyll. Scale bar: 5 µm. (D) Western blots of whole-cell lysates (5 µg protein per lane) of *bld1 IFT52::3HA*, *bld1* and *bld1 IFT46::YFP IFT52::3HA* (*bld1 IFT46 IFT52*) probed with the indicated antibodies. IB, immunoblot. (E) Western blots of whole-cell lysates (5 µg protein per lane) of *bld1 IFT52::3HA*, *bld1* and *bld1 IFT46-C1::YFP IFT52::3HA* (*bld1 IFT46-C1 IFT52*) probed with the indicated antibodies. IB, immunoblot. (F) Confocal imaging of *bld1* expressing IFT46::YFP IFT52::3HA or IFT46-C1::YFP IFT52::3HA. CHL, chlorophyll. Scale bar: 5 µm. (G) Western blots of whole-cell lysates (5 µg protein per lane) of *ift46-1 IFT46::YFP* (*ift46-1 IFT46*), *ift46-1* and *ift46-1 IFT52::YFP* (*ift46-1 IFT52*) probed with the indicated antibodies. IB, immunoblot. # labels individual transformants in A,B,D,E,G. (H) Confocal images of *ift46-1* expressing IFT52::YFP. CHL, chlorophyll. Scale bar: 5 µm.

NLS-tagged IFT52C recruits IFT46 to nuclei

IFT46-C1 is necessary and sufficient for the basal body and ciliary targeting of IFT46 (Figs 2–4), and IFT52 binds to and recruits IFT46-C1 to the basal body (Figs 5, 6). It is also known that some IFT46 associates with cytoplasmic vesicles and is then delivered to the basal body region in *C. reinhardtii* (Wood and Rosenbaum, 2014). However, there are still two possibilities regarding the molecular mechanism of the basal body targeting of IFT46. One is that IFT52 is delivered to the basal body first and recruits the free IFT46 to form a complex at the basal body. The interaction between IFT46 and IFT52 only occurs at the basal body region. The other is that newly synthesized IFT46 and IFT52 preassemble as subcomplexes, and that these subcomplexes are delivered to the basal body region. The key difference between these two scenarios is the location of where IFT46 assembles with IFT52. One possibility is that it occurs around the basal body and the other is that it happens in the TGN or cytoplasm. To rule out one of these possibilities, we aimed to localize IFT52 in nuclei and examine whether IFT46 follows.

There are various nuclear localization signals or sequences (NLSs) in animal and plant cells (Kropat et al., 2005; Lange et al., 2007; Rasala et al., 2014). However, only a few have been reported in *C. reinhardtii* (Kropat et al., 2005; Rasala et al., 2014). We attached NLSs from simian virus 40 (SV40; two copies , 2×SV40; and four copies, 4×SV40), copper response regulator 1 and nucleoplasmin to the C-terminus of YFP and expressed them in WT cells. Notably, only 4×SV40 NLS worked efficiently to bring the YFP into nuclei (Fig. 7B; data not shown). For the sake of simplicity, NLS hereafter refers to the 4×SV40 NLS. Given that it has been previously reported that the C-terminus of IFT52 (IFT52C) interacts with IFT46 (Lucker et al., 2010; Taschner et al., 2011, 2014) and that overexpression of the C-terminus of *Mus musculus* IFT52 has a strong dominant-negative effect on ciliogenesis in MDCK cells, which may be caused by the mislocalization of other

Journal of Cell Science (2017) 130, 1662-1674 doi:10.1242/jcs.200758

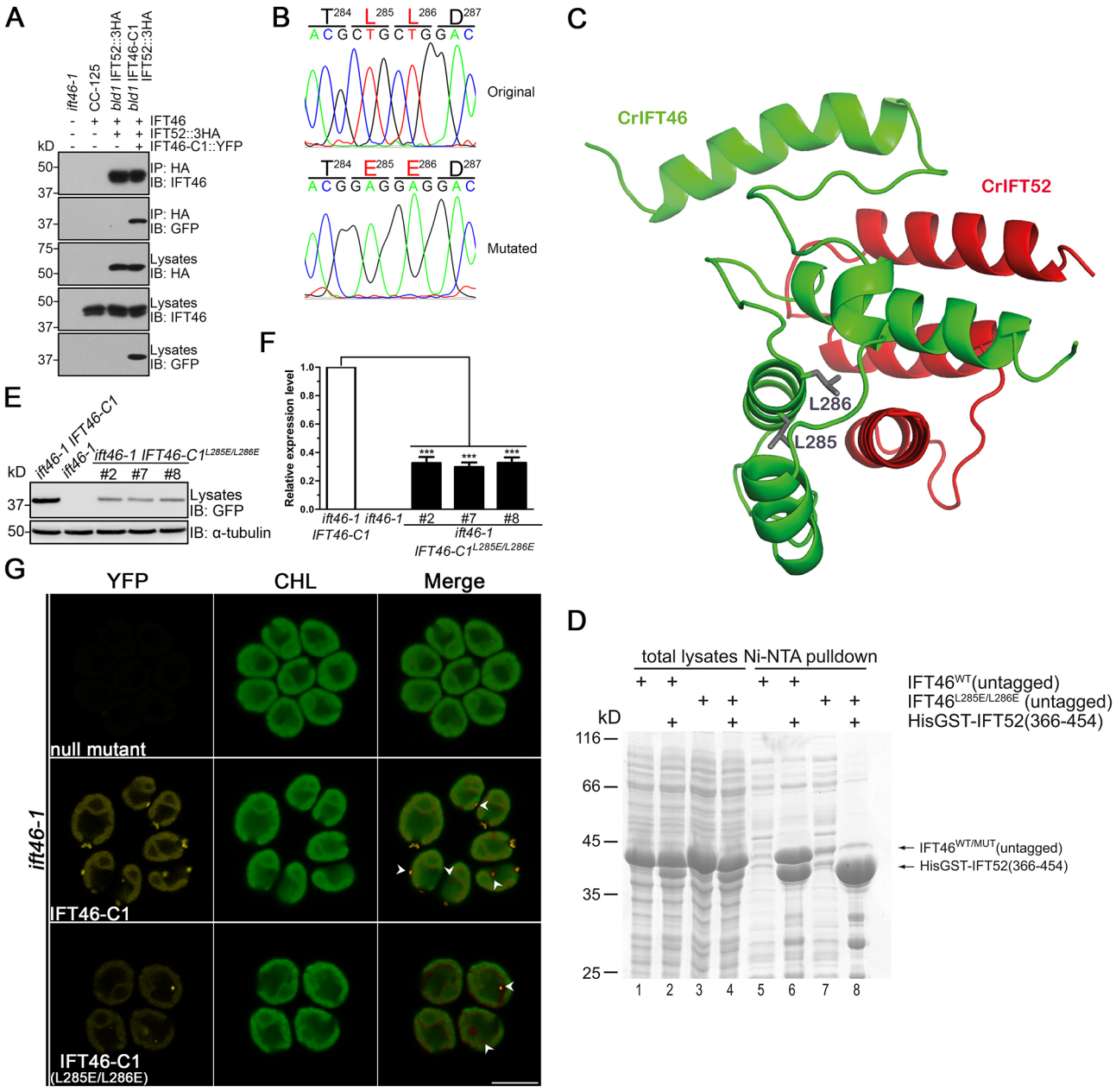

Fig. 6. IFT52 binds to and recruits IFT46 to the basal body. (A) An antibody against HA was used to immunoprecipitate HA-tagged IFT52 from whole-cell lysates of *ift46-1*, CC-125, *bld1 IFT52::3HA* and *bld1 IFT46-C1 IFT52::3HA*. Immunoblots of the precipitates were probed with antibodies as indicated. IP, immunoprecipitation; IB, immunoblot. (B) Schematic diagram of site-directed mutagenesis of the *IFT46* gene. The upper panel shows the original DNA and protein sequence while the lower panel displays the mutated one. (C) Model of *C. reinhardtii* (Cr)IFT52C–IFT46C based on the *Tetrahymena thermophile* IFT52C–IFT46C crystal structure (PDB ID: 4UZZ). The two residues we chose for mutagenesis are highlighted as gray sticks. (D) Pull-down of His-tagged GST::IFT52(366-454) with untagged WT IFT46 or IFT46$^{L285E/L286E}$ coexpressed in *E. coli* demonstrates that double point mutations are sufficient to disrupt the interaction between IFT46 and IFT52. The weak band in the area where IFT46^{WT} or IFT46$^{L285E/L286E}$ ran (Fig. 6D, lane 8) was due to non-specific binding of the IFT46 protein to the beads (as it was also present in the control, lane 7). Numbers at the bottom indicate lanes. (E) Western blots of whole-cell lysates (3 µg protein per lane) of *ift46-1 IFT46::YFP*, *ift46-1* and *ift46-1* expressing YFP-tagged *IFT46-C1$^{L285E/L286E}$* probed with the indicated antibodies. IB, immunoblot. (F) Relative expression levels of IFT46-C1$^{L285E/L286E}$ in three transformants (2, 7 or 8) compared to the expression level of IFT46-C1. Values are shown as the mean±s.e.m. of five independent experiments. Statistical analysis was performed using one-way ANOVA followed by Tukey's test. ***P<0.001. (G) Confocal imaging of non-transformed cells of *ift46-1* and *ift46-1* expressing IFT46-C1::YFP or IFT46-C1$^{L285E/L286E}$::YFP. White arrowheads, eyespots; CHL, chlorophyll. Scale bar: 10 µm.

IFT-B subunits (Taschner et al., 2014), we chose to fuse IFT52C to the NLS. In WT cells, positive transformants expressing IFT52C::YFP::NLS were identified using immunoblotting with an antibody against GFP (Fig. 7A). Using confocal imaging, we found that the fusion protein IFT52C::YFP::NLS was enriched in nuclei successfully, just as YFP::NLS was (Fig. 7B), which was also apparent from immunoblotting of nuclear lysates (Fig. 7C). Likewise, IFT46 was detected in nuclear lysates of CC-125 *IFT52C::YFP::NLS* (Fig. 7C). This was further verified by immunostaining, which revealed IFT46 colocalized with IFT52C::YFP::NLS in nuclei of CC-125 *IFT52C::YFP::NLS* (Fig. 7D). We also found that IFT52C immunoprecipitated with IFT46 in nuclear lysates of CC-125 *IFT52C::YFP::NLS* (Fig. 7E). These data demonstrate that IFT46 can be recruited ectopically to

Journal of Cell Science (2017) 130, 1662-1674 doi:10.1242/jcs.200758

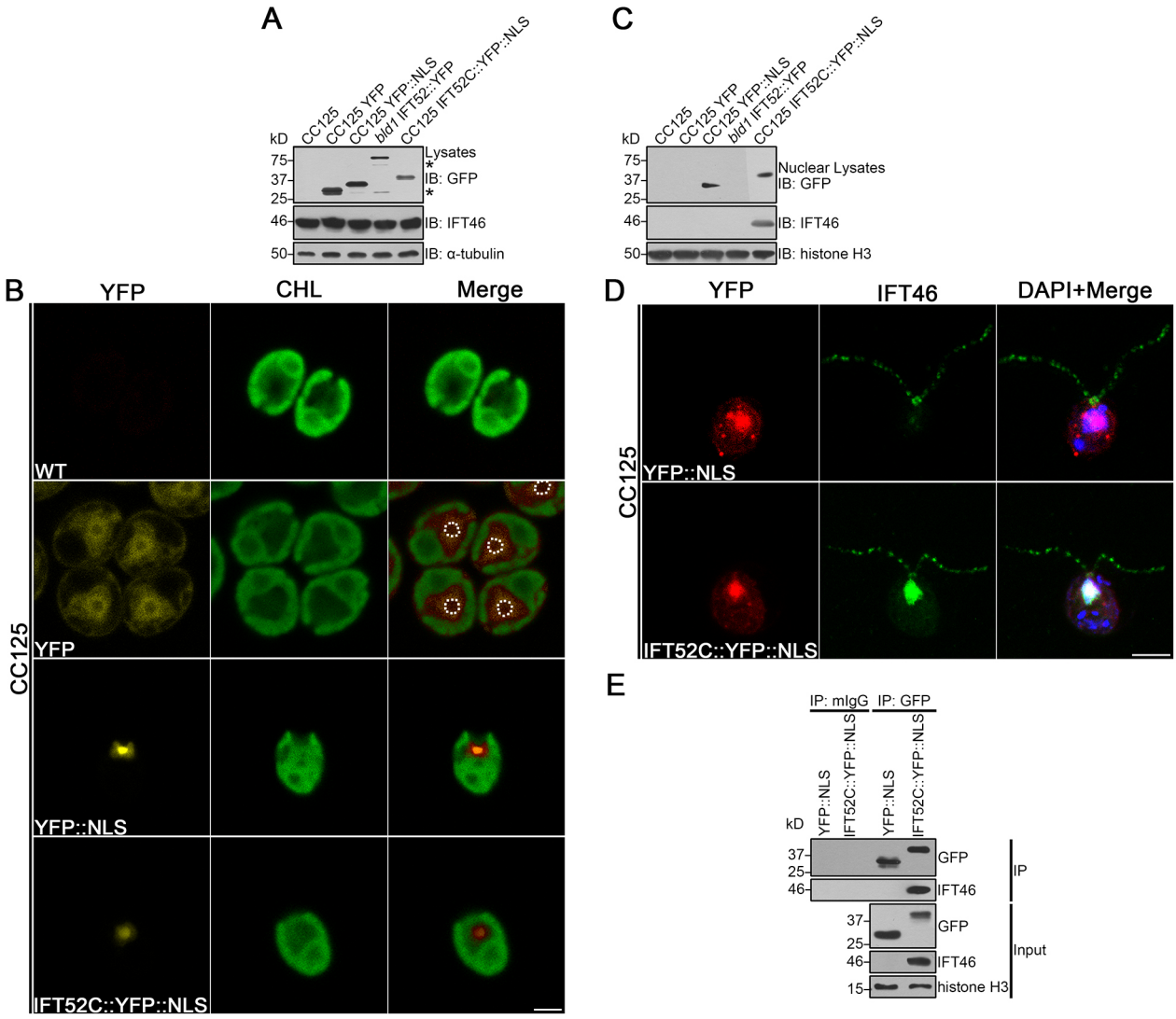

Fig. 7. NLS-tagged IFT52C recruits IFT46 to nuclei. (A) Western blots of whole-cell lysates (5 µg protein per lane) of CC-125, CC-125 *YFP*, CC-125 *YFP::NLS*, *bld1 IFT52::YFP* and CC-125 *IFT52C::YFP::NLS* probed with the indicated antibodies. IB, immunoblot. (B) Live-cell imaging of WT cells and WT cells expressing YFP, YFP::NLS and IFT52C::YFP::NLS. White dashed circles mark the nucleus area. CHL, chlorophyll. Scale bar: 5 µm. (C) Western blots of nuclear lysates (2 µg protein per lane) of CC-125, CC-125 *YFP*, CC-125 *YFP::NLS*, *bld1 IFT52::YFP* and CC-125 *IFT52C::YFP::NLS* probed with the indicated antibodies. IB, immunoblot. (D) Immunofluorescence microscopy of CC-125 *YFP::NLS* and CC-125 *IFT52C::YFP::NLS* using antibodies against GFP (red) and IFT46 (green), and nuclei were stained with DAPI (blue). Scale bar: 5 µm. (E) An antibody against GFP was used to immunoprecipitate (IP) IFT52C::YFP::NLS from the nuclei of CC-125 *IFT52C::YFP::NLS*. mIgG, mouse IgG.

nuclei by NLS-fused IFT52C, which indicates that they have been preassembled in the cytoplasm and not at the basal body.

DISCUSSION

Cilia are evolutionarily conserved organelles. Ciliogenesis and ciliary sensory functions rely on IFT. Although IFT was described more than 20 years ago (Kozminski et al., 1993), the mechanism of basal body localization of the IFT complex has remained elusive. Our data demonstrate that the C-terminus of IFT46 is indispensable for its basal body targeting. IFT52 binds to and recruits IFT46 to the basal body. The assembly of IFT52 and IFT46 can occur in the nucleus ectopically. These results suggest that they are preassembled in the cytoplasm or in the TGN, not at the basal body (Fig. 8). During flagellar regeneration in *Chlamydomonas*, IFT46 has been observed in TGN-derived vesicles (Wood and Rosenbaum, 2014), and it is possible that IFT52 and IFT46 are preassembled in the TGN and are delivered to the basal body through vesicular transport (Fig. 8). However, only IFT20 has been show to be localized in the Golgi, and most IFT proteins are not associated with the membrane (Follit et al., 2006; Richey and Qin, 2012). Thus, the possibility that IFT52–IFT46 are preassembled in the cytoplasm and then targeted to the basal body through non-vesicle-mediated means cannot be ruled out (Fig. 8).

IFT46-C1 cannot be regarded as the basal body- and ciliary-targeting sequence of IFT46 because IFT46-C1 directly interacts with IFT52, which is the putative targeting carrier of IFT46 (Figs 4, 5). IFT46-C1 can no longer accumulate in basal bodies when this interaction is disrupted by mutating two important consensus residues to glutamic acid (Fig. 5). However, the interaction partner of IFT46 is still an IFT subunit, IFT52 (Fig. 6). This indicates that – unlike the third intracellular loop of different GPCRs, the Ax(S/A)xQ and RVxP motifs, NLSs or SUMOylation – IFT46-C1 is not a general or 'classic' basal body targeting sequence or signal (Bhogaraju et al., 2013; Dishinger et al., 2010; Malicki and

Journal of Cell Science (2017) 130, 1662-1674 doi:10.1242/jcs.200758

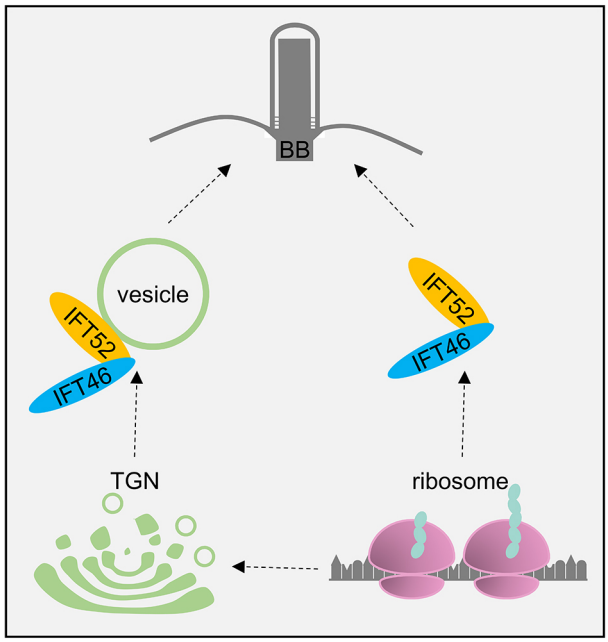

Fig. 8. Model for basal body localization of IFT46. Newly synthesized IFT52 and IFT46 from the ribosome are preassembled in the cytoplasm and are delivered to the basal body in a non-vesicle-mediated manner. A second scenario is that IFT52 and IFT46 are preassembled in the TGN and are targeted to the basal body through a vesicle-mediated pathway. BB, basal body.

Avidor-Reiss, 2014; McIntyre et al., 2015). Future work should be performed to identify the 'real' targeting sequence in IFT52 or other upstream IFT proteins.

The IFT machinery has at least 22 members (Taschner and Lorentzen, 2016; Taschner et al., 2016). They all accumulate at the basal body. One simple model would be that all IFT proteins are translated at ribosomes and assembled at the basal body. However, IFT46 and IFT52 could assemble in the nucleus when the C-terminus of IFT52 was ectopically expressed in nuclei. Therefore, these data do not support that model. Another possibility is that IFT proteins preassemble as a small subcomplex before their translocation to and localization at the basal body. Our results here support this latter scenario. In fact, Brown et al. have found that IFT-A colocalizes with IFT-B within the basal body IFT pool in the WT but not in *ift74-1* (Brown et al., 2015). These results imply that IFT-A and IFT-B are targeted to basal bodies independently. Our speculation matches observations that IFT-A localizes normally to the basal body in null mutants of IFT-B and that IFT-B proteins localize normally in null mutants of IFT-A components (Behal et al., 2012; Brown et al., 2015; Hou et al., 2007; Richey and Qin, 2012). Furthermore, CPLANE proteins can regulate the basal body recruitment of peripheral IFT-A complexes but not of IFT-A core or IFT-B complexes (Toriyama et al., 2016). Future work is required to determine how many IFT subcomplexes are assembled before targeting to the basal body and whether IFT cargos are recruited before these subcomplexes reach the basal body. These studies will pave the way for the deciphering of the mechanism of interaction between the IFT proteins, motors and cargos at the basal body.

MATERIALS AND METHODS

Algal strains and culture conditions

The *C. reinhardtii* strains used in this study are listed in Table S1. The strains CC-125, *ift46-1*, *bld1*, *ift88*, *fla10-2* and *dhc1b* were obtained from the *Chlamydomonas* Resource Center, University of Minnesota. Strains *ift81-2* and *ift122-1* were a gift from Professor Junmin Pan at Tisinghua University in China.

The *Chlamydomonas* cells were grown in liquid Tris-acetate-phosphate (TAP) (Harris et al., 1989) or minimal (MI) (Sager and Granick, 1953) media at 22°C with constant agitation and illumination (about 25 µE m^{-2} s^{-1}) in 96-well plates, 250 ml Erlenmeyer flasks or 5 l aerated glass containers (Hu et al., 2014). For long-term storage, the *Chlamydomonas* cells were maintained on solid TAP medium supplemented with 1.5% agar at 20°C with a cycle of 14 h of light and 10 h of dark.

Primers and plasmid construction

To rescue the null mutant of *ift46-1*, two plasmids (pHK214 and pHK266) expressing IFT46::YFP were constructed. Firstly, the genomic DNA of the *IFT46* gene was amplified from pGEM T Easy-*IFT46* with primers IFT46-F and IFT46-R. The 4 kb PCR fragment was then cloned into pMD 18-T vector (TaKaRa, Japan) yielding pHK212. After digestion with *Nde*I and *Eco*RV, the *IFT46* gene in pHK212 was subcloned into the corresponding restriction sites of pHK86, giving rise to pHK214. pHK214 was then digested with *Eco*RI and filled with the klenow fragment of DNA polymerase I; the linearized and blunt-ended pHK214 was then digested with *Kpn*I. A 2.3 kb fragment from pHK265 between the *StuI* and *KpnI* restriction sites, including selectable marker gene *AphVII*, was inserted in the blunt and *Kpn*I sites of pHK214, resulting in pHK266. To create a vector expressing only YFP, a fragment was amplified from pHK214 using the primers ACE-F and Pro-R. This fragment was cleaved with *Nde*I and *Eco*RV. The resultant fragment was cloned into *Nde*I-*Eco*RV-digested pHK214, creating pHK281.

To rescue the null mutant of *IFT52*, *bld1*, three plasmids – pHK250 (expressing IFT52::YFP), pHK268 (expressing IFT52::YFP) and pHK409 (expressing IFT52::3HA) – were created. The genomic DNA of *IFT52* was amplified using primers IFT52A-F and IFT52B-R with the genomic DNA of CC503 as the template. After cleavage by *Nde*I and *Eco*RV, the genomic DNA fragment was ligated into *Nde*I-*Eco*RV-digested pHK86 or pHK266, yielding pHK250 and PHK268, respectively. To fuse a 3×HA tag to the C-terminus of IFT52, four oligonucleotides (HA1, HA2, HA3 and HA4) were annealed, and the resultant fragment was inserted in frame into *Eco*RV-*Eco*RI-digested pHK250, resulting in pHK409.

In order to express truncated versions of IFT46, pHK231, pHK232, pHK233, pHK243, pHK244 and pHK245 were constructed. These vectors express IFT46-N1, IFT46-N, IFT46ΔC1, IFT46ΔN1, IFT46-C and IFT46-C1 in *C. reinhardtii*, respectively. *IFT46-N1* was amplified with primers ACE-F and A-R using pGEM-T Easy-*IFT46* as the template. The PCR products were trimmed with *Nde*I and *Eco*RV and inserted into *Nde*I-*Eco*RV-digested pHK86, resulting in pHK231. The expression vectors of IFT46-N (pHK232) and IFT46ΔC1 (pHK233) were constructed just as pHK231, except using primer sets ACE-F and C-R, and ACE-F and E-R, respectively. To obtain the coding sequence of IFT46ΔN1, two elements, the promoter of *IFT46* and the coding sequence of IFT46ΔN1, were needed. The promoter of *IFT46* was amplified with primers ACE-F and B-R using pGEM-T Easy-*IFT46* as the template. The coding fragment of IFT46ΔN1 was also amplified using pGEM-T Easy-*IFT46* as the template with primers B-F and IFT46-R. These two elements formed an overlap and were then cut with *Nde*I and *Eco*RV. The digested fragment was ligated into *Nde*I-*Eco*RV-cleaved pHK86, giving rise to pHK243. The construction procedures for pHK244 (expressing IFT46-C) and pHK245 (expressing IFT46-C1) were similar to those of pHK243 using different primers. Primer pairs ACE-F and D-R, and ACE-F and F-R were used to amplify the promoter of *IFT46* for pHK244 and pHK245, respectively. Their coding fragments were obtained using D-F and IFT46-R, and F-F and IFT46-R, respectively.

To express truncated versions of IFT46-C1, pHK308, pHK310, pHK309, pHK311, pHK312 and pHK313 were constructed. These vectors encode BBTS1, BBTS3, BBTS2, BBTS4, BBTS5 and BBTS6, respectively. *BBTS1* was amplified using primers BBTS-F and BBTS1-R with pHK245 as the template. The PCR products were cut with *Nde*I and *Eco*RV and then cloned back into *Nde*I-*Eco*RV-digested pHK245, yielding pHK308. The plasmid expressing BBTS3, pHK310, was constructed in a similar way using primers BBTS-F and BBTS3-R. To create pHK309, expressing BBTS2, an overlap was created between the promoter sequence of *IFT46* (amplified from

Journal of Cell Science (2017) 130, 1662-1674 doi:10.1242/jcs.200758

pHK245 using primers BBTS-F and BBTS2-R) and the coding region of BBTS2 (amplified from pHK245 using primers BBTS2-F and IFT46-R). Then, the overlapped PCR products were digested with *Nde*I and *Eco*RV and subcloned into pHK245. The cloning procedures for pHK311 (expressing BBTS4), pHK312 (expressing BBTS5) and pHK313 (expressing BBTS6) were identical to those for pHK309. To amplify the promoter sequence of *IFT46* for pHK311, pHK312 and pHK313, primer sets BBTS-F and BBTS4-R, BBTS-F and BBTS5-R1, and BBTS-F and BBTS6-R were used, respectively. To obtain the coding sequence of BBTS4, five oligonucleotides (BBTS4-1, BBTS4-2, BBTS4-3, BBTS4-4 and BBTS4-5) were annealed together. To amplify the coding region of BBTS5, primers BBTS5-F and BBTS5-R2 were used. The coding DNA of BBTS6 was generated using similar procedures to that for BBTS4. Thus, it was created by annealing BBTS6-6, BBTS6-7, BBTS4-2, BBTS4-3 and BBTS4-5.

To construct pHK464 expressing YFP::NLS, the second *YFP* gene in pHK469 was removed by digestion with *Eco*RV and *Eco*RI and replaced by 4×SV40 NLS (4×DPKKKRKV). The 4×SV40 NLS was obtained by annealing five oligonucleotides, namely 4×NLS-1F, 4×NLS-2R, 4×NLS-3F, 4×NLS-4R and 4×NLS-5R. The *YFP-NLS* fragment in pHK464 was amplified with primers NLS-F and NLS-R. The PCR products were trimmed with *Sma*I and *Eco*RI, and cloned into *Eco*RV-*Eco*RI-digested pHK409, giving rise to pHK470. To further create pHK473 expressing IFT52C::YFP::NLS, a fragment was amplified in an inverse PCR from pHK470 with primers IFT52C-F and IFT52C-R. The purified inverse PCR products were assembled seamlessly using the In-Fusion HD cloning method (Clontech, #639648, Japan).

All plasmids and primers used in this work are listed in Tables S2 and S3, respectively. All constructs were verified by sequencing (Shenggong Inc., China).

Site-directed mutagenesis

The fragment of *IFT46-C1* was cut out from pHK245 with *Nde*I and *Eco*RV, and cloned into *Nde*I-*Eco*RV-digested pHK266, resulting in pHK242. In order to disrupt the protein–protein interaction between IFT46-C1 and IFT52, pHK242, which encodes IFT46-C1, was mutated using Fast Mutagenesis System (TRANS, #FM111-01) with primers SDM-F and SDM-R, generating pHK267. When expressed, the critical binding sites of IFT46-C1 with IFT52, namely leucine residues 285 and 286, were replaced with glutamic acid residues.

Measurement of flagellar length

The cells were fixed with 0.5% Lugol's solution for 2 min at room temperature. Flagellar lengths were measured under a phase microscope (Nikon Eclipse Ti) equipped with an electron-multiplying charge-coupled device. For each sample, at least 50 cells and 100 flagella were measured.

Bioinformatic analysis

The genomic DNA and protein sequences of *IFT46* and *IFT52* were retrieved from *C. reinhardtii* v5.5 database in Joint Genome Institute Phytozome 11. The protein sequences of IFT46 of *Volvox carteri f. nagariensis* (XP_002950030), *Homo sapiens* (NP_001162089), *Mus musculus* (NP_076320), *Caenorhabditis elegans* (NP_001076770), *Xenopus laevis* (NP_001090393), *Bos taurus* (NP_001068677), *Canis lupus familiaris* (XP_536553), *Rattus norvegicus* (NP_001019931), *Gallus gallus* (XP_417918), *Danio rerio* (XP_003199413), *Strongylocentrotus purpuratus* (XP_795443), *Schistosoma japonicum* (Q5DHJ5), *Emiliania huxleyi* (XP_005763582), *Tetrahymena thermophila* (XP_001017111) and *Apis mellifera* (XP_006565024) were obtained from National Center for Biotechnology Information (NCBI). Multiple sequence alignment was performed by ClustalX2.0 (Larkin et al., 2007).

The secondary structures of IFT46 were predicted by PSIPRED (Buchan et al., 2013). The protein disorder of IFT46 was analyzed using GeneSilico Metadisorder (Kozlowski and Bujnicki, 2012). The crystal structure data of *T. thermophila* IFT52C–IFT46C was downloaded from RCSB Protein Data Bank (ID: 4UZZ). The three-dimensional structure of *C. reinhardtii* IFT52C–IFT46C was modeled based on *T. thermophila* IFT52C–IFT46C using the server Phyre2 (Kelley et al., 2015; Taschner et al., 2014).

Electro-transformation of *C. reinhardtii*

Plasmids were linearized by *Nde*I or *Sca*I before electro-transformation. Electroporation was performed as described previously (Brown et al., 1991; Hu et al., 2014; Shimogawara et al., 1998).

Protein extraction and quantification

Whole-cell soluble proteins were extracted as described previously (Fowkes and Mitchell, 1998; Hu et al., 2014). Nuclear proteins were extracted with CelLytic PN Plant Nuclei Isolation/Extraction Kit (Sigma-Aldrich, #CELLYTPN1) according to the manufacturer's guidelines. The protein concentration was determined by using the Amido black 10B binding method with BSA as a standard (Hu et al., 2014; Schaffner and Weissmann, 1973).

Flagellar isolation and fractionation

Flagella were isolated using pH shock, as previously described (Cole et al., 1998; Witman et al., 1972). For membrane-plus-matrix and axonemal fractionation, the flagellar pellets were dissolved in HMDEK buffer containing 0.5% NP-40. The suspension was rotated for 20 min at 4°C and centrifuged at 10,000 ***g*** for 10 min at 4°C. The supernatant and pellet were membrane-plus-matrix and axonemal fractions, respectively.

SDS-PAGE and immunoblotting assay

SDS-PAGE and immunoblotting assays were performed as previously described (Hu et al., 2014). Primary and secondary antibodies used in this study are listed in Table S4. For quantification of the signals of immunoblotting, the developed films were scanned and analyzed using Adobe Photoshop CS6.

Pull-down assay

C. reinhardtii IFT46 (WT or mutant) and *C. reinhardtii* IFT52C constructs were transformed either alone or in combination in *E. coli* BL21(DE3). Proteins were expressed and purified as reported previously (Taschner et al., 2016). GST pulldown assays were performed as previously described (Taschner et al., 2016).

Sucrose density gradient centrifugation

Sucrose density gradient centrifugation of flagellar membrane-plus-matrix fraction was performed as described previously (Behal and Cole, 2013). Firstly, insoluble materials in the flagellar membrane-plus-matrix fraction were removed by centrifugation twice at 100,000 ***g*** for 10 min at 4°C. Then, 150 µl of supernatant was loaded on top of 10–25% sucrose density gradients. This 5 ml ultracentrifuge tube was centrifuged at 200,000 ***g*** for 4.5 h at 4°C in the MLS-50 rotor (Optima-XP Ultracentrifuge, Beckman Coulter). The resulting gradients were fractioned into 200 µl aliquots. Aliquots were analyzed by SDS-PAGE and immunoblotting.

Immunofluorescence staining

Immunofluorescence staining of *Chlamydomonas* cells were performed as detailed previously (Engel et al., 2012). If needed, 5 µg/ml DAPI in PBS was used for the washing steps. The antibodies used for immunofluorescence staining are given in Table S4.

Immunoprecipitation

Immunoprecipitation was performed as described by Richey and Qin (2013).

Nucleus isolation

Nuclei of *Chlamydomonas* were isolated using an optimized method, as described previously (Winck et al., 2011) with one additional step. Specifically, the cell pellets were digested with autolysin for 1 h at room temperature before cryogenic grinding with liquid nitrogen.

RNA preparation and quantitative real-time PCR

Total RNA was isolated using TRIzol reagent (Invitrogen). cDNA was generated through reverse transcription using First Strand cDNA Synthesis Kit with oligo(dT)$_{18}$ primers (Thermo Scientific). Quantitative real-time

PCR was performed with the Applied Biosystems 7900HT Fast Real-Time PCR System according to the manufacturer's instructions using SYBR Green Realtime PCR Master Mix (TOYOBO). *CBLP* served as the control. For *IFT46*, primer pair 2 was used. For *CBLP*, primers CBLP-F and CBLP-R were used (Table S3).

Microscopy

Live-cell imaging of *Chlamydomonas* was performed on an NLS-LSM710 confocal laser-scanning microscope (Carl Zeiss, Germany) using a 63× oil objective lens (NA 1.40). The excitation/emission parameters were as follows: chlorophyll, 488/560–580 nm; YFP, 512/515–560 nm; CFP, 458/459–530 nm. Images of immunostained samples were obtained on a Leica TCS SP8 confocal microscope equipped with a 63× oil-immersion lens (NA 1.40). The excitation/emission parameters were as follows: DAPI, 405/423–488 nm; FITC, 488/495–545 nm; Alexa-Fluor-594, 552/612–671 nm. Brightness and contrast were adjusted using Carl Zeiss Zen 2009 Light Edition, Leica LAS AF 2.6.3, or ImageJ 1.46r software.

IFT measurements

Visualization and recording of IFT were performed according to published protocols (Engel et al., 2012; Lechtreck, 2013, 2016). Videos were recorded using a Nikon Eclipse Ti total internal reflection fluorescence microscope. This microscope was equipped with a cooled electron-multiplying charge-coupled device, a 100× oil objective lens (NA 1.49) and a 514 nm laser with a 540 nm bandpass (30 nm) filter.

Statistical analysis

Statistical results were obtained from at least three independent experiments. All data are reported as mean±s.e.m. Differences between groups were tested by analysis of variance using Student's *t*-test or one-way ANOVA followed by Tukey's test using Prism 5.01 (GraphPad Software). Differences were considered significant when P was less than 0.05. Asterisks represent P-values of <0.05 (*), <0.01 (**) and <0.001 (***).

Acknowledgements

We thank Junmin Pan for kindly providing the null mutants *ift81-2* and *ift122*. We thank Gai Liu for help with the amplification of the genomic DNA of *IFT52*. We thank Kangsup Yoon, Jinliang Liu, Keke Zhang and Wei Li for their comments and suggestions that improved the manuscript.

Competing interests

The authors declare no competing or financial interests.

Author contributions

B.L. designed and performed research, analyzed data and wrote the manuscript; L.W., M.T. and X.C. designed and performed research; L.W., M.T. and X.C. contributed to design and editing of the manuscript; E.L. and K.H. supervised and designed research, analyzed data and wrote the manuscript.

Funding

This work was supported by grants to K.H. from National Natural Science Foundation of China (grant 31371354) and to E.L. from the Novo Nordisk Foundation (grant NNF15OC0014164).

Supplementary information

Supplementary information available online at
http://jcs.biologists.org/lookup/doi/10.1242/jcs.200758.supplemental

References

Ahmed, N. T., Gao, C., Lucker, B. F., Cole, D. G. and Mitchell, D. R. (2008). ODA16 aids axonemal outer row dynein assembly through an interaction with the intraflagellar transport machinery. *J. Cell. Biol.* **183**, 313-322.

Baldari, C. T. and Rosenbaum, J. (2010). Intraflagellar transport: it's not just for cilia anymore. *Curr. Opin. Cell. Biol.* **22**, 75-80.

Behal, R. H. and Cole, D. G. (2013). Analysis of interactions between intraflagellar transport proteins. *Method. Enzymol.* **524**, 171-194.

Behal, R. H., Miller, M. S., Qin, H., Lucker, B. F., Jones, A. and Cole, D. G. (2012). Subunit interactions and organization of the *Chlamydomonas reinhardtii* intraflagellar transport complex A proteins. *J. Biol. Chem.* **287**, 11689-11703.

Berbari, N. F., Johnson, A. D., Lewis, J. S., Askwith, C. C. and Mykytyn, K. (2008). Identification of ciliary localization sequences within the third intracellular loop of G protein-coupled receptors. *Mol. Biol. Cell.* **19**, 1540-1547.

Bhogaraju, S., Engel, B. D. and Lorentzen, E. (2013). Intraflagellar transport complex structure and cargo interactions. *Cilia* **2**, 10.

Blacque, O. E., Reardon, M. J., Li, C., McCarthy, J., Mahjoub, M. R., Ansley, S. J., Badano, J. L., Mah, A. K., Beales, P. L. and Davidson, W. S. (2004). Loss of *C. elegans* BBS-7 and BBS-8 protein function results in cilia defects and compromised intraflagellar transport. *Genes. Dev.* **18**, 1630-1642.

Borovina, A. and Ciruna, B. (2013). IFT88 plays a cilia-and PCP-independent role in controlling oriented cell divisions during vertebrate embryonic development. *Cell. Rep.* **5**, 7.

Breslow, D. K., Koslover, E. F., Seydel, F., Spakowitz, A. J. and Nachury, M. V. (2013). An in vitro assay for entry into cilia reveals unique properties of the soluble diffusion barrier. *J. Cell. Biol.* **203**, 129-147.

Brooks, E. R. and Wallingford, J. B. (2012). Control of vertebrate intraflagellar transport by the planar cell polarity effector Fuz. *J. Cell. Biol.* **198**, 37-45.

Brooks, E. R. and Wallingford, J. B. (2013). The small GTPase Rsg1 is important for the cytoplasmic localization and axonemal dynamics of intraflagellar transport proteins. *Cilia* **2**, 13.

Brown, L. E., Sprecher, S. L. and Keller, L. R. (1991). Introduction of exogenous DNA into *Chlamydomonas reinhardtii* by electroporation. *Mol. Cell. Biol.* **11**, 2328-2332.

Brown, J. M., Cochran, D. A., Craige, B., Kubo, T. and Witman, G. B. (2015). Assembly of IFT trains at the ciliary base depends on IFT74. *Curr. Biol.* **25**, 1583-1593.

Buchan, D. W. A., Minneci, F., Nugent, T. C. O., Bryson, K. and Jones, D. T. (2013). Scalable web services for the PSIPRED protein analysis workbench. *Nuleic Acids Res.* **41**, W349-W357.

Cole, D. G., Diener, D. R., Himelblau, A. L., Beech, P. L., Fuster, J. C. and Rosenbaum, J. L. (1998). *Chlamydomonas* kinesin-II–dependent intraflagellar transport (IFT): IFT particles contain proteins required for ciliary assembly in *Caenorhabditis elegans* sensory neurons. *J. Cell. Biol.* **141**, 993-1008.

Deane, J. A., Cole, D. G., Seeley, E. S., Diener, D. R. and Rosenbaum, J. L. (2001). Localization of intraflagellar transport protein IFT52 identifies basal body transitional fibers as the docking site for IFT particles. *Curr. Biol.* **11**, 1586-1590.

Dishinger, J. F., Kee, H. L., Jenkins, P. M., Fan, S., Hurd, T. W., Hammond, J. W., Truong, Y. N.-T., Margolis, B., Martens, J. R. and Verhey, K. J. (2010). Ciliary entry of the kinesin-2 motor KIF17 is regulated by importin-beta2 and RanGTP. *Nat. Cell. Biol.* **12**, 703-710.

Engel, B. D., Ishikawa, H., Wemmer, K. A., Geimer, S., Wakabayashi, K.-i., Hirono, M., Craige, B., Pazour, G. J., Witman, G. B. and Kamiya, R. (2012). The role of retrograde intraflagellar transport in flagellar assembly, maintenance, and function. *J. Cell. Biol.* **199**, 151-167.

Fan, Z.-C., Behal, R. H., Geimer, S., Wang, Z., Williamson, S. M., Zhang, H., Cole, D. G. and Qin, H. (2010). *Chlamydomonas* IFT70/CrDYF-1 is a core component of IFT particle complex B and is required for flagellar assembly. *Mol. Biol. Cell.* **21**, 2696-2706.

Fliegauf, M., Benzing, T. and Omran, H. (2007). When cilia go bad: cilia defects and ciliopathies. *Nat. Rev. Mol. Cell. Biol.* **8**, 880-893.

Follit, J. A., Tuft, R. A., Fogarty, K. E. and Pazour, G. J. (2006). The intraflagellar transport protein IFT20 is associated with the Golgi complex and is required for cilia assembly. *Mol. Biol. Cell.* **17**, 3781-3792.

Fowkes, M. E. and Mitchell, D. R. (1998). The role of preassembled cytoplasmic complexes in assembly of flagellar dynein subunits. *Mol. Biol. Cell.* **9**, 2337-2347.

Gerdes, J. M., Davis, E. E. and Katsanis, N. (2009). The vertebrate primary cilium in development, homeostasis, and disease. *Cell* **137**, 32-45.

Goetz, S. C., Liem, K. F., Jr and Anderson, K. V. (2012). The spinocerebellar ataxia-associated gene Tau tubulin kinase 2 controls the initiation of ciliogenesis. *Cell* **151**, 847-858.

Griesbeck, O., Baird, G. S., Campbell, R. E., Zacharias, D. A. and Tsien, R. Y. (2001). Reducing the environmental sensitivity of yellow fluorescent protein. Mechanism and applications. *J. Biol. Chem.* **276**, 29188-29194.

Griffiths, G. M., Tsun, A. and Stinchcombe, J. C. (2010). The immunological synapse: a focal point for endocytosis and exocytosis. *J. Cell. Biol.* **189**, 399-406.

Harris, E. H., Stern, D. B. and Witman, G. (1989). *The Chlamydomonas Sourcebook*. San Diego, USA: Academic Press.

Hildebrandt, F. and Zhou, W. (2007). Nephronophthisis-associated ciliopathies. *J. Am. Soc. Nephrol.* **18**, 1855-1871.

Hildebrandt, F., Benzing, T. and Katsanis, N. (2011). Ciliopathies. *N. Engl. J. Med.* **364**, 1533-1543.

Hou, Y., Pazour, G. J. and Witman, G. B. (2004). A dynein light intermediate chain, D1bLIC, is required for retrograde intraflagellar transport. *Mol. Biol. Cell.* **15**, 4382-4394.

Hou, Y., Qin, H., Follit, J. A., Pazour, G. J., Rosenbaum, J. L. and Witman, G. B. (2007). Functional analysis of an individual IFT protein: IFT46 is required for transport of outer dynein arms into flagella. *J. Cell. Biol.* **176**, 653-665.

Hu, J., Deng, X., Shao, N., Wang, G. and Huang, K. (2014). Rapid construction and screening of artificial microRNA systems in *Chlamydomonas reinhardtii*. *Plant. J.* **79**, 1052-1064.

Hurd, T. W., Fan, S. and Margolis, B. L. (2011). Localization of retinitis pigmentosa 2 to cilia is regulated by Importin β2. *J. Cell. Sci.* **124**, 718-726.

Inaba, M., Buszczak, M. and Yamashita, Y. M. (2015). Nanotubes mediate niche-stem-cell signalling in the *Drosophila* testis. *Nature* **523**, 329-332.

Ishikawa, H. and Marshall, W. F. (2011). Ciliogenesis: building the cell's antenna. *Nat. Rev. Mol. Cell. Biol.* **12**, 222-234.
Jones, D. T. (1999). Protein secondary structure prediction based on position-specific scoring matrices. *J. Mol. Biol.* **292**, 195-202.
Joo, K., Kim, C. G., Lee, M.-S., Moon, H.-Y., Lee, S.-H., Kim, M. J., Kweon, H.-S., Park, W.-Y., Kim, C.-H., Gleeson, J. G. et al. (2013). CCDC41 is required for ciliary vesicle docking to the mother centriole. *Proc. Natl. Acad. Sci. USA* **110**, 5987-5992.
Kelley, L. A., Mezulis, S., Yates, C. M., Wass, M. N. and Sternberg, M. J. E. (2015). The Phyre2 web portal for protein modeling, prediction and analysis. *Nat. Protoc.* **10**, 845-858.
Kozlowski, L. P. and Bujnicki, J. M. (2012). MetaDisorder: a meta-server for the prediction of intrinsic disorder in proteins. *BMC Bioinformatics* **13**, 111.
Kozminski, K. G., Johnson, K. A., Forscher, P. and Rosenbaum, J. L. (1993). A motility in the eukaryotic flagellum unrelated to flagellar beating. *Proc. Natl. Acad. Sci. USA* **90**, 5519-5523.
Kozminski, K. G., Beech, P. L. and Rosenbaum, J. L. (1995). The *Chlamydomonas* kinesin-like protein FLA10 is involved in motility associated with the flagellar membrane. *J. Cell. Biol.* **131**, 1517-1527.
Kropat, J., Tottey, S., Birkenbihl, R. P., Depege, N., Huijser, P. and Merchant, S. (2005). A regulator of nutritional copper signaling in *Chlamydomonas* is an SBP domain protein that recognizes the GTAC core of copper response element. *Proc. Natl. Acad. Sci. USA* **102**, 18730-18735.
Lange, A., Mills, R. E., Lange, C. J., Stewart, M., Devine, S. E. and Corbett, A. H. (2007). Classical nuclear localization signals: definition, function, and interaction with importin alpha. *J. Biol. Chem.* **282**, 5101-5105.
Larkin, M. A., Blackshields, G., Brown, N. P., Chenna, R., McGettigan, P. A., McWilliam, H., Valentin, F., Wallace, I. M., Wilm, A., Lopez, R. et al. (2007). Clustal W and Clustal X version 2.0. *Bioinformatics* **23**, 2947-2948.
Lechtreck, K. F. (2013). In vivo imaging of IFT in *Chlamydomonas* flagella. *Method. Enzymol.* **524**, 265.
Lechtreck, K. F. (2016). Methods for studying movement of molecules within cilia. *Methods Mol. Biol.* **1454**, 83-96.
Long, H. and Huang, K. (2012). Analysis of flagellar protein ubiquitination. *Method. Enzymol.* **524**, 59-73.
Lucker, B. F., Behal, R. H., Qin, H., Siron, L. C., Taggart, W. D., Rosenbaum, J. L. and Cole, D. G. (2005). Characterization of the intraflagellar transport complex B core: direct interaction of the IFT81 and IFT74/72 subunits. *J. Biol. Chem.* **280**, 27688-27696.
Lucker, B. F., Miller, M. S., Dziedzic, S. A., Blackmarr, P. T. and Cole, D. G. (2010). Direct interactions of intraflagellar transport complex B proteins IFT88, IFT52, and IFT46. *J. Biol. Chem.* **285**, 21508-21518.
Malicki, J. and Avidor-Reiss, T. (2014). From the cytoplasm into the cilium: bon voyage. *Organogenesis* **10**, 138-157.
McIntyre, J. C., Joiner, A. M., Zhang, L., Iniguez-Lluhi, J. and Martens, J. R. (2015). SUMOylation regulates ciliary localization of olfactory signaling proteins. *J. Cell. Sci.* **128**, 1934-1945.
Miller, M. S., Esparza, J. M., Lippa, A. M., Lux, F. G., Cole, D. G. and Dutcher, S. K. (2005). Mutant kinesin-2 motor subunits increase chromosome loss. *Mol. Biol. Cell.* **16**, 3810-3820.
Mizuno, N., Taschner, M., Engel, B. D. and Lorentzen, E. (2012). Structural studies of ciliary components. *J. Mol. Biol.* **422**, 163-180.
Mourão, A., Christensen, S. T. and Lorentzen, E. (2016). The intraflagellar transport machinery in ciliary signaling. *Curr. Opin. Struct. Biol.* **41**, 98-108.
Ou, G., Blacque, O. E., Snow, J. J., Leroux, M. R. and Scholey, J. M. (2005). Functional coordination of intraflagellar transport motors. *Nature* **436**, 583-587.
Pan, X., Ou, G., Civelekoglu-Scholey, G., Blacque, O. E., Endres, N. F., Tao, L., Mogilner, A., Leroux, M. R., Vale, R. D. and Scholey, J. M. (2006). Mechanism of transport of IFT particles in *C. elegans* cilia by the concerted action of kinesin-II and OSM-3 motors. *J. Cell. Biol.* **174**, 1035-1045.
Pazour, G. J., Dickert, B. L. and Witman, G. B. (1999). The DHC1b (DHC2) isoform of cytoplasmic dynein is required for flagellar assembly. *J. Cell. Biol.* **144**, 473-481.
Pedersen, L. B. and Rosenbaum, J. L. (2008). Intraflagellar transport (IFT) role in ciliary assembly, resorption and signalling. *Curr. Top. Dev. Biol.* **85**, 23-61.
Pigino, G., Geimer, S., Lanzavecchia, S., Paccagnini, E., Cantele, F., Diener, D. R., Rosenbaum, J. L. and Lupetti, P. (2009). Electron-tomographic analysis of intraflagellar transport particle trains in situ. *J. Cell. Biol.* **187**, 135-148.
Rasala, B. A., Chao, S.-S., Pier, M., Barrera, D. J. and Mayfield, S. P. (2014). Enhanced genetic tools for engineering multigene traits into green algae. *PLoS ONE* **9**, e94028.
Richey, E. A. and Qin, H. (2012). Dissecting the sequential assembly and localization of intraflagellar transport particle complex B in *Chlamydomonas*. *PLoS ONE* **7**, e43118.
Richey, E. A. and Qin, H. (2013). Isolation of intraflagellar transport particle proteins from *Chlamydomonas reinhardtii*. *Method. Enzymol.* **524**, 1-17.
Sager, R. and Granick, S. (1953). Nutritional studies with *Chlamydomonas reinhardtii*. *Ann. N.Y. Acad. Sci.* **56**, 831-838.
Santos, N. and Reiter, J. F. (2014). A central region of Gli2 regulates its localization to the primary cilium and transcriptional activity. *J. Cell Sci.* **127**, 1500-1510.
Satir, P. and Christensen, S. T. (2007). Overview of structure and function of mammalian cilia. *Annu. Rev. Physiol.* **69**, 377-400.
Schaffner, W. and Weissmann, C. (1973). A rapid, sensitive, and specific method for the determination of protein in dilute solution. *Anal. Biochem.* **56**, 502-514.
Scholey, J. M. (2003). Intraflagellar transport. *Annu. Rev. Cell Dev. Biol.* **19**, 423-443.
Shimogawara, K., Fujiwara, S., Grossman, A. and Usuda, H. (1998). High-efficiency transformation of *Chlamydomonas reinhardtii* by electroporation. *Genetics* **148**, 1821-1828.
Singla, V. and Reiter, J. F. (2006). The primary cilium as the cell's antenna: signaling at a sensory organelle. *Science* **313**, 629-633.
Snow, J. J., Ou, G., Gunnarson, A. L., Walker, M. R. S., Zhou, H. M., Brust-Mascher, I. and Scholey, J. M. (2004). Two anterograde intraflagellar transport motors cooperate to build sensory cilia on *C. elegans* neurons. *Nat. Cell Biol.* **6**, 1109-1113.
Stepanek, L. and Pigino, G. (2016). Microtubule doublets are double-track railways for intraflagellar transport trains. *Science* **352**, 721-724.
Taschner, M. and Lorentzen, E. (2016). The intraflagellar transport machinery. *Cold Spring Harb. Perspect. Biol.* **8**, a028092.
Taschner, M., Bhogaraju, S., Vetter, M., Morawetz, M. and Lorentzen, E. (2011). Biochemical mapping of interactions within the intraflagellar transport (IFT) B core complex IFT52 binds directly to four other IFT-B subunits. *J. Biol. Chem.* **286**, 26344-26352.
Taschner, M., Kotsis, F., Braeuer, P., Kuehn, E. W. and Lorentzen, E. (2014). Crystal structures of IFT70/52 and IFT52/46 provide insight into intraflagellar transport B core complex assembly. *J. Cell Biol.* **207**, 269-282.
Taschner, M., Weber, K., Mourão, A., Vetter, M., Awasthi, M., Stiegler, M., Bhogaraju, S. and Lorentzen, E. (2016). Intraflagellar transport proteins 172, 80, 57, 54, 38, and 20 form a stable tubulin-binding IFT-B2 complex. *EMBO J.* **35**, 773-790.
Toriyama, M., Lee, C., Taylor, S. P., Duran, I., Cohn, D. H., Bruel, A.-L., Tabler, J. M., Drew, K., Kelly, M. R., Kim, S. et al. (2016). The ciliopathy-associated CPLANE proteins direct basal body recruitment of intraflagellar transport machinery. *Nat. Genet.* **48**, 648-656.
Vannuccini, E., Paccagnini, E., Cantele, F., Gentile, M., Dini, D., Fino, F., Diener, D., Mencarelli, C. and Lupetti, P. (2016). Two classes of short intraflagellar transport train with different 3D structures are present in *Chlamydomonas* flagella. *J. Cell Sci.* **129**, 2064-2074.
Walther, Z., Vashishtha, M. and Hall, J. L. (1994). The *Chlamydomonas FLA10* gene encodes a novel kinesin-homologous protein. *J. Cell Biol.* **126**, 175-188.
Winck, F. V., Kwasniewski, M., Wienkoop, S. and Mueller-Roeber, B. (2011). An optimized method for the isolation of nuclei from *Chlamydomonas reinhardtii* (Chlorophyceae). *J. Phycol.* **47**, 333-340.
Witman, G. B., Carlson, K., Berliner, J. and Rosenbaum, J. L. (1972). *Chlamydomonas* flagella. I. Isolation and electrophoretic analysis of microtubules, matrix, membranes, and mastigonemes. *J. Cell Biol.* **54**, 507-539.
Wood, C. R. and Rosenbaum, J. L. (2014). Proteins of the ciliary axoneme are found on cytoplasmic membrane vesicles during growth of cilia. *Curr. Biol.* **24**, 1114-1120.
Wood, C. R. and Rosenbaum, J. L. (2015). Ciliary ectosomes: transmissions from the cell's antenna. *Trends. Cell Biol.* **25**, 276-285.
Wood, C. R., Wang, Z., Diener, D., Zones, J. M., Rosenbaum, J. and Umen, J. G. (2012). IFT proteins accumulate during cell division and localize to the cleavage furrow in *Chlamydomonas*. *PLoS ONE* **7**, e30729.
Ye, X., Zeng, H., Ning, G., Reiter, J. F. and Liu, A. (2014). C2cd3 is critical for centriolar distal appendage assembly and ciliary vesicle docking in mammals. *Proc. Natl. Acad. Sci. USA* **111**, 2164-2169.

Figures

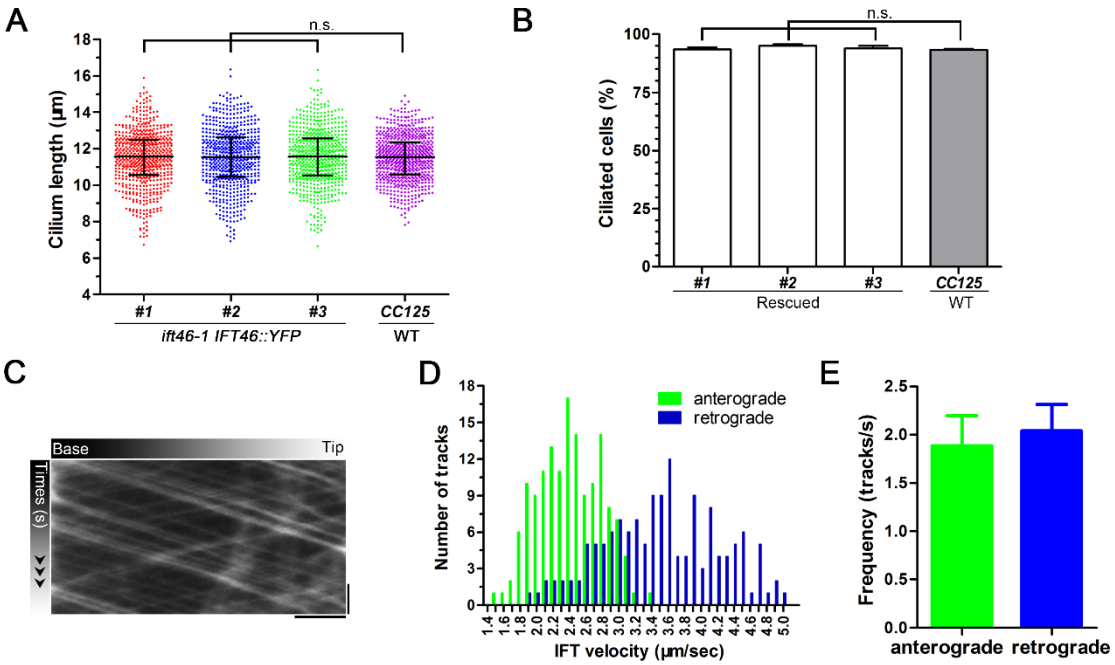

Fig. S1. YFP-tagged IFT46 rescued the flagellar defects in *ift46-1*.

(A) Flagella length of rescued strain *ift46-1 IFT46::YFP* is nearly identical to that of WT cells. At least 100 flagella per experiment (n=6) were measured. Scatter plots show the median, the upper and the lower quartiles. Dots represent individual data points.

(B) Percentages of ciliated cells of WT and the rescued strains *ift46-1 IFT46::YFP*. At least 100 cells per experiment (n=6) were measured. Values are shown as the mean ± s.e.m. Statistical analysis was performed using one-way ANOVA followed by Turkey test. n.s.: not significant.

(C) A typical kymograph generated from an image stack of flagella of *ift46-1 IFT46::YFP* showed anterograde and retrograde tracks. The horizontal axis matches the length of one flagellum while the vertical axis corresponds to the passed time. Horizontal scale bar: 2 µm; vertical scale bar: 2 s.

(D) Frequency distribution of anterograde IFT velocity (green bar, n=149) and retrograde IFT velocity (blue bar, n=145) of *ift46-1 IFT46::YFP*.

(E) IFT frequencies obtained from kymographs of image stacks (for anterograde frequency, n = 21; for retrograde frequency, n = 20).

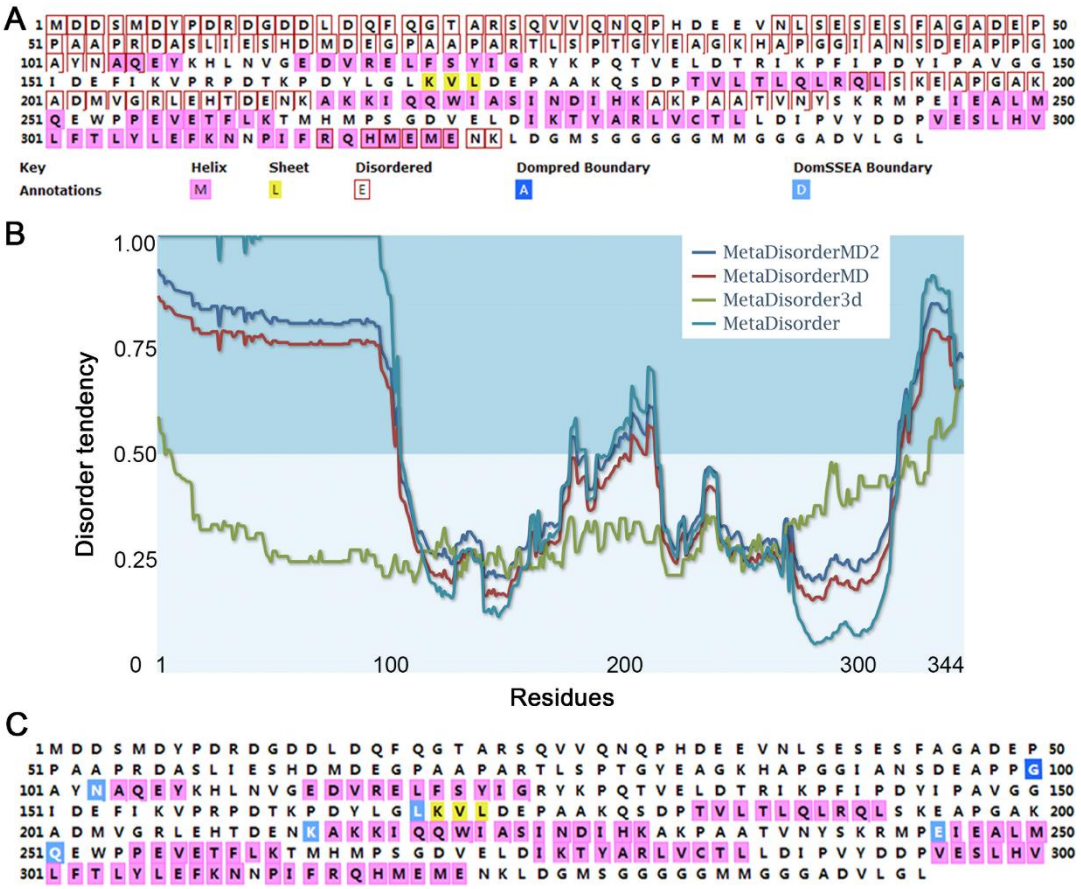

Fig. S2. Advanced structure predictions of IFT46.

(A) Secondary structure prediction of IFT46. Meanings of symbols were given below.

(B) Protein disorder prediction indicates that the N-terminus and the C-terminus tail of IFT46 are largely disordered. The line at 0.5 (vertical axis) is the cutoff for disorder (> 0.5) and order (< 0.5) predictions. Curved lines with different colors represent results returned by four different meta method as shown.

(C) Domain prediction of IFT46 using PSIPRED DomPred. Potential domain boundaries were shown in colored boxes.

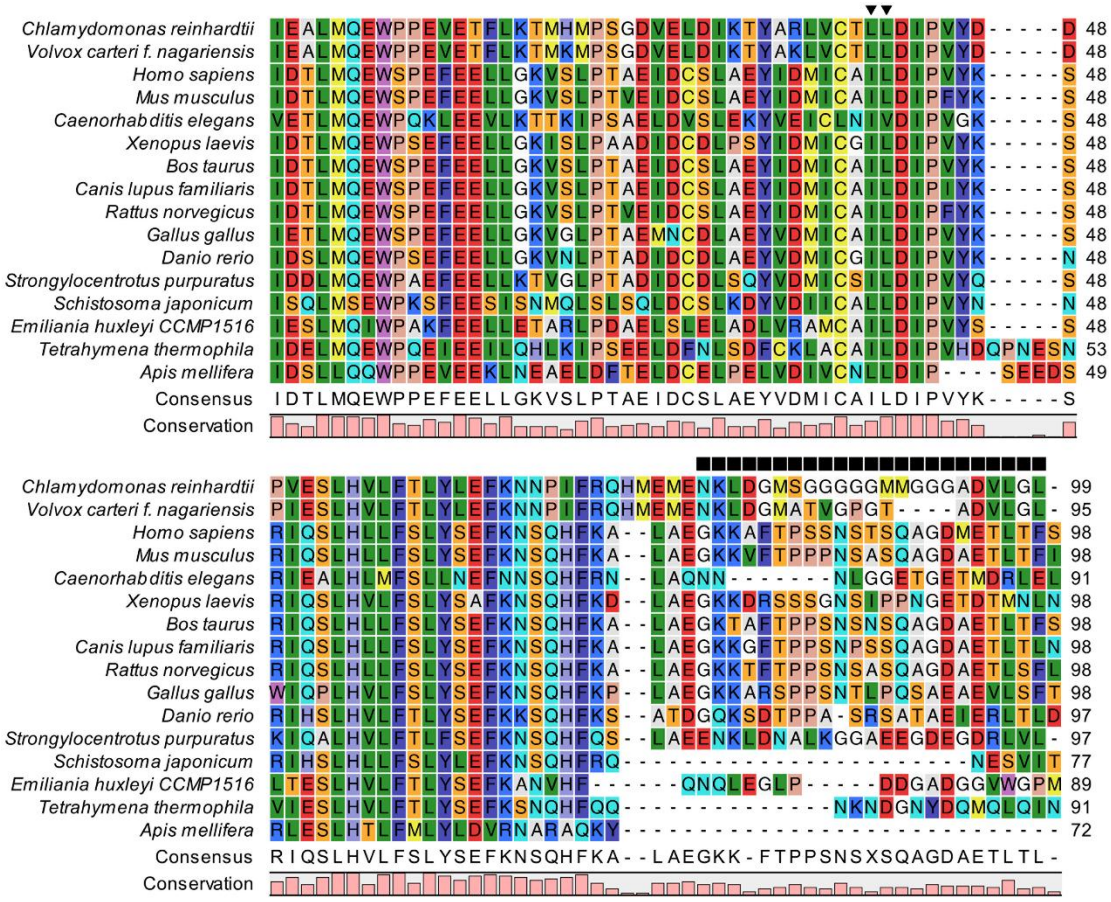

Fig. S3. IFT46-C1 is highly conserved in evolution.

The amino acid sequences of IFT46-C1 from indicated species were aligned. The black triangles mark the two critical hydrophobic leucines we chosen for mutagenesis. The black squares mark the glycine-rich tail of CrIFT46. The consensus sequence and the graph showing percentages of conservation are given at the bottom.

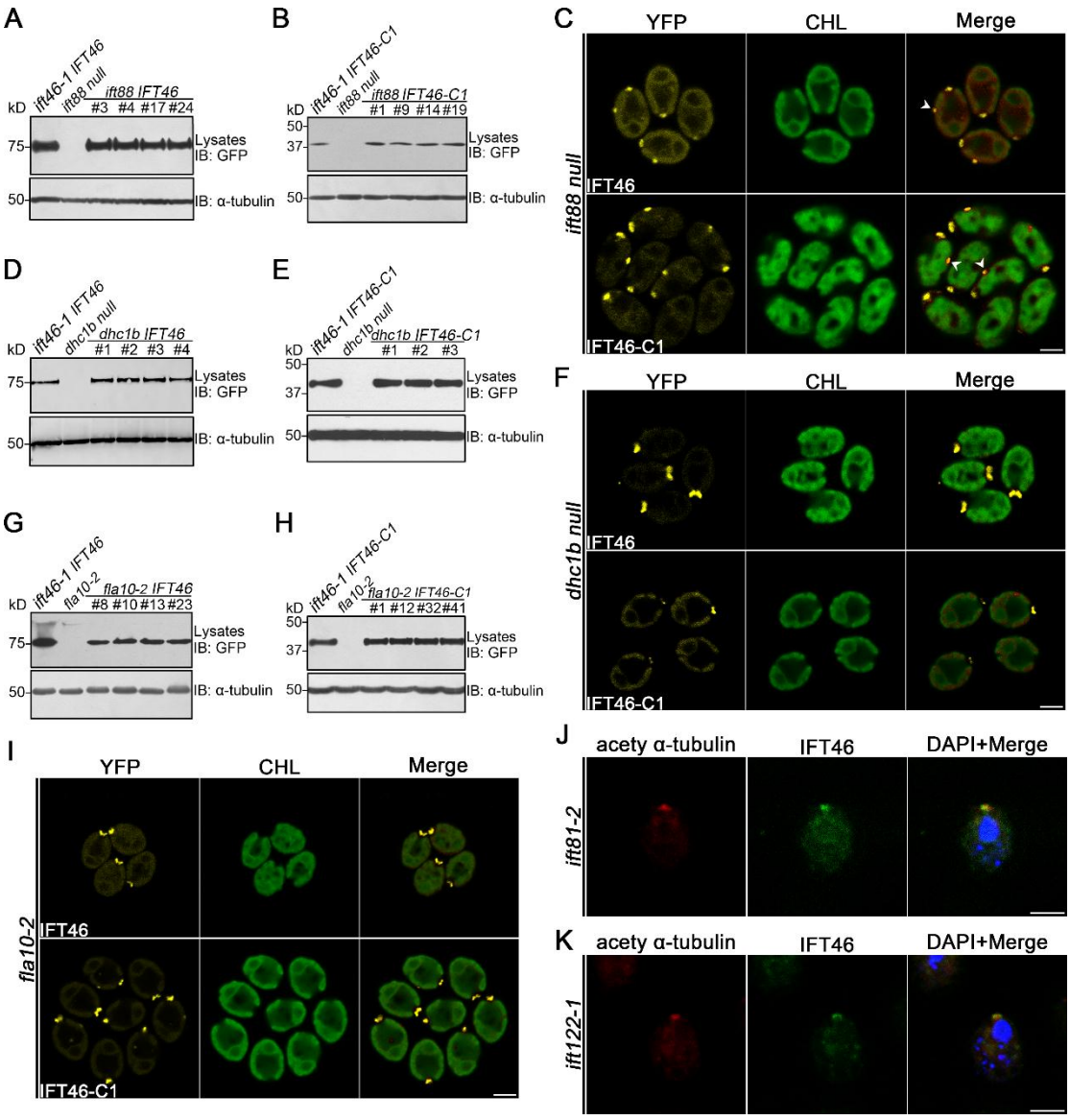

Fig. S4. The basal body localization of IFT46 is independent of IFT122, IFT88, IFT81, FLA10 or DHC1b.

(A) Western blots of whole-cell lysates (5 µg protein per lane) of *ift46-1 IFT46::YFP*, *ift88* null, and *ift88 IFT46::YFP* probed with the indicated antibodies. IB: immunoblot.

(B) Western blots of whole-cell lysates (5 µg protein per lane) of *ift46-1 IFT46-C1::YFP*, *ift88* null, and *ift88 IFT46-C1::YFP* probed with the indicated antibodies. IB: immunoblot.

(C) Confocal imaging of *ift88* null mutant expressing IFT46::YFP or IFT46-C1::YFP. White arrows mark the eyespots. CHL: chlorophyll.

(D) Western blots of whole-cell lysates (5 µg protein per lane) of *ift46-1 IFT46::YFP*, *dhc1b* null, and *dhc1b IFT46::YFP* probed with the indicated antibodies. IB: immunoblot.

(E) Western blots of whole-cell lysates (5 µg protein per lane) of *ift46-1 IFT46-C1::YFP*,

dhc1b null, and *dhc1b IFT46-C1::YFP* probed with the indicated antibodies. IB: immunoblot.

(F) Confocal imaging of *dhc1b* null mutant expressing IFT46::YFP or IFT46-C1::YFP. CHL: chlorophyll.

(G) Western blots of whole-cell lysates (5 µg protein per lane) of *ift46-1 IFT46::YFP*, *fla10-2*, and *fla10-2 IFT46::YFP* probed with the indicated antibodies. IB: immunoblot.

(H) Western blots of whole-cell lysates (5 µg protein per lane) of *ift46-1 IFT46-C1::YFP*, *fla10-2*, and *fla10-2 IFT46-C1::YFP* probed with the indicated antibodies. IB: immunoblot.

(I) Confocal imaging of *fla10-2* expressing IFT46::YFP or IFT46-C1::YFP. CHL: chlorophyll.

(J) Immunostaining of *ift81-2* using anti-acetylated α-tubulin antibody (red), anti-IFT46 antibody (green) and DAPI (blue).

(K) Immunostaining of *ift122-1* using anti-acetylated α-tubulin antibody (red), anti-IFT46 antibody (green) and DAPI (blue).

In panel C, F, I and J, scale bars represent 5 µm.

Tables

Table S1

Click here to Download Table S1

Table S2. Plasmids used in this study.

Plasmid Number	Relevant Genotype or usage[a]	Source
pGEM-T Easy-*IFT46*	pIFT46, *AMP^R*	Dr. Joel Rosenbaum
pHK212	pIFT46::YFP, *AMP^R*	this study
pHK214	pIFT46::YFP, *AMP^R PRM^R*	this study
pHK231	pIFT46-N1::YFP, *AMP^R PRM^R*	this study
pHK232	pIFT46-N::YFP, *AMP^R PRM^R*	this study
pHK233	pIFT46ΔC1::YFP, *AMP^R PRM^R*	this study
pHK242	pIFT46-C1::YFP, *AMP^R HYG^R*	this study
pHK243	pIFT46ΔN1::YFP, *AMP^R PRM^R*	this study
pHK244	pIFT46-C::YFP, *AMP^R PRM^R*	this study
pHK245	pIFT46-C1::YFP, *AMP^R PRM^R*	this study
pHK265	*AMP^R HYG^R*	this study
pHK266	pIFT46::YFP, *AMP^R HYG^R*	this study
pHK267	pIFT46-C1$^{L285E/L286E}$::YFP, *AMP^R HYG^R*	this study
pHK268	pIFT52::YFP, *AMP^R HYG^R*	this study
pHK281	pYFP, *AMP^R PRM^R*	this study
pHK308	pBBTS1::YFP, *AMP^R PRM^R*	this study
pHK309	pBBTS2::YFP, *AMP^R PRM^R*	this study
pHK310	pBBTS3::YFP, *AMP^R PRM^R*	this study
pHK311	pBBTS4::YFP, *AMP^R PRM^R*	this study
pHK312	pBBTS5::YFP, *AMP^R PRM^R*	this study
pHK313	pBBTS6::YFP, *AMP^R PRM^R*	this study
pHK409	pIFT52::3HA, *AMP^R PRM^R*	this study
pHK464	pYFP::NLS, *AMP^R PRM^R*	this study
pHK473	pIFT52C::YFP::NLS, *AMP^R PRM^R*	this study
pHK86	pGFP-YFP, *AMP^R PRM^R*	(Long and Huang, 2012)
pHK87	pGFP-CFP, *AMP^R PRM^R*	(Long and Huang, 2012)

pHK250	pIFT52::YFP, *AMP*^{R} *PRM*^{R}	this study
pHK469	pYFP::YFP, *AMP*^{R} *PRM*^{R}	this study
pHK470	pIFT52::YFP::NLS, *AMP*^{R} *PRM*^{R}	this study
pHyg3	*HYG*^{R}	Dr. Wolfgang Mages
pMD18-T	for TA cloning, *AMP*^{R}	TaKaRa Bio Inc.

[a]*AMP*^{R}, ampicillin resistance; *PRM*^{R}, paromomycin resistance; *HYG*^{R}, hygromycin B resistance

Table S3

Click here to Download Table S3

Table S4. Antibodies used in this study.

Immunogen	Biological source	Dilution Factor	Note and Source
acetylated α-tubulin	mouse	1: 1000	Sigma, #T6793
GFP	mouse	1: 1000	Roche, #11814460001
GFP	mouse	1: 5000	Abmart, #M20004
HA	rabbit	1: 5000	Roche, #11867423001
histone H3	rabbit	1: 5000	Agrisera, #AS10710
IFT46	rabbit	1: 5000	Prepared by Genscript using the N-terminal 20 amino-acids peptide and purified using the same peptide
IFT52	rabbit	1: 250	(Deane et al., 2001)
IFT74	rabbit	1: 2500	(Qin et al., 2004)
IFT81	mouse	1: 250	(Lucker et al., 2005)
mIgG	goat	1: 500	Alexa Fluor 488 conjugated, Life technologies, A-11029
mIgG	goat	1: 5000	HRP conjugated, Sigma-Aldrich, #A4416
rIgG	goat	1: 500	Alexa Fluor 594 conjugated, Life technologies, #A-11037
rIgG	goat	1: 5000	HRP conjugated, Life technologies, #G21234
rIgG	goat	1: 5000	HRP conjugated, Sigma-Aldrich, #6154
α-tubulin	mouse	1: 200000	Sigma-Aldrich, #T9026

Movies

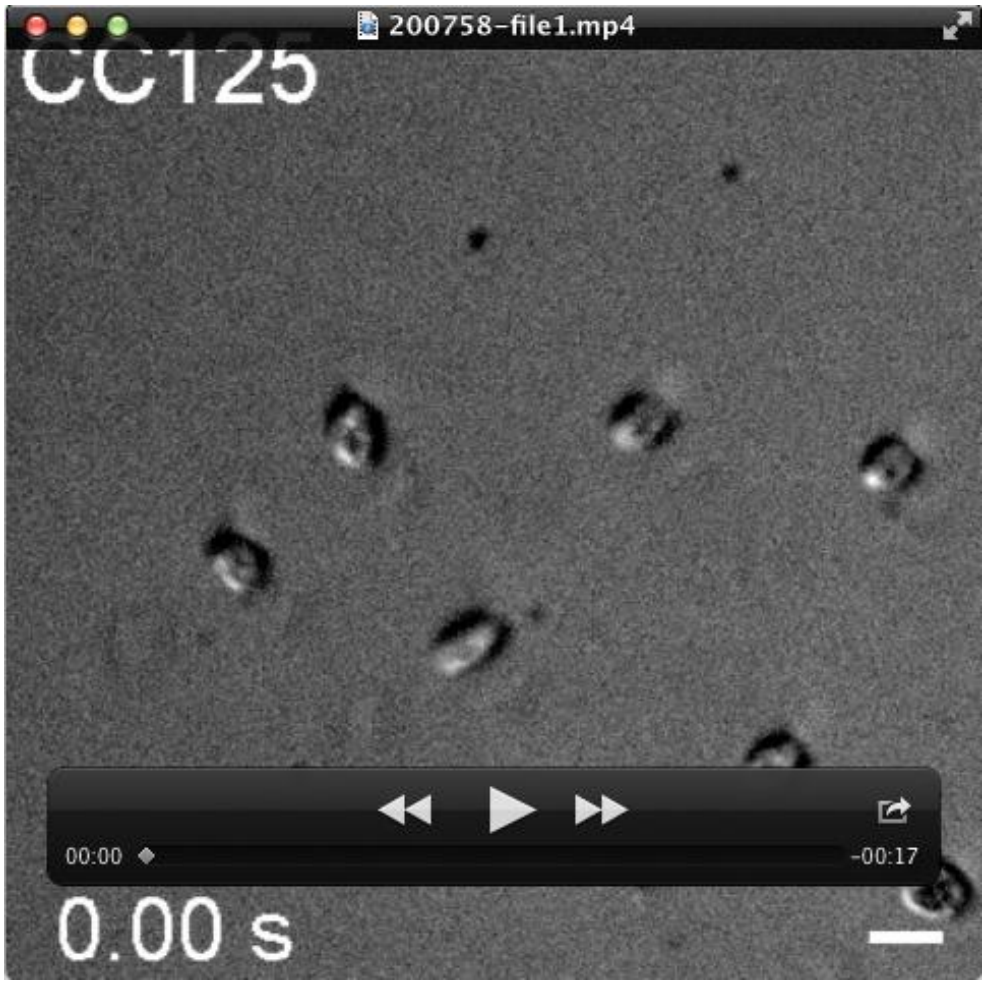

Movie 1 Locomotion of WT cells.

A representative movie taken for WT cells. Scale bar: 10 μm. Images were observed under a DIC microscope with a 100x objective, recorded at one frame per 0.13 sec and displayed as it is.

Journal of Cell Science • Supplementary information

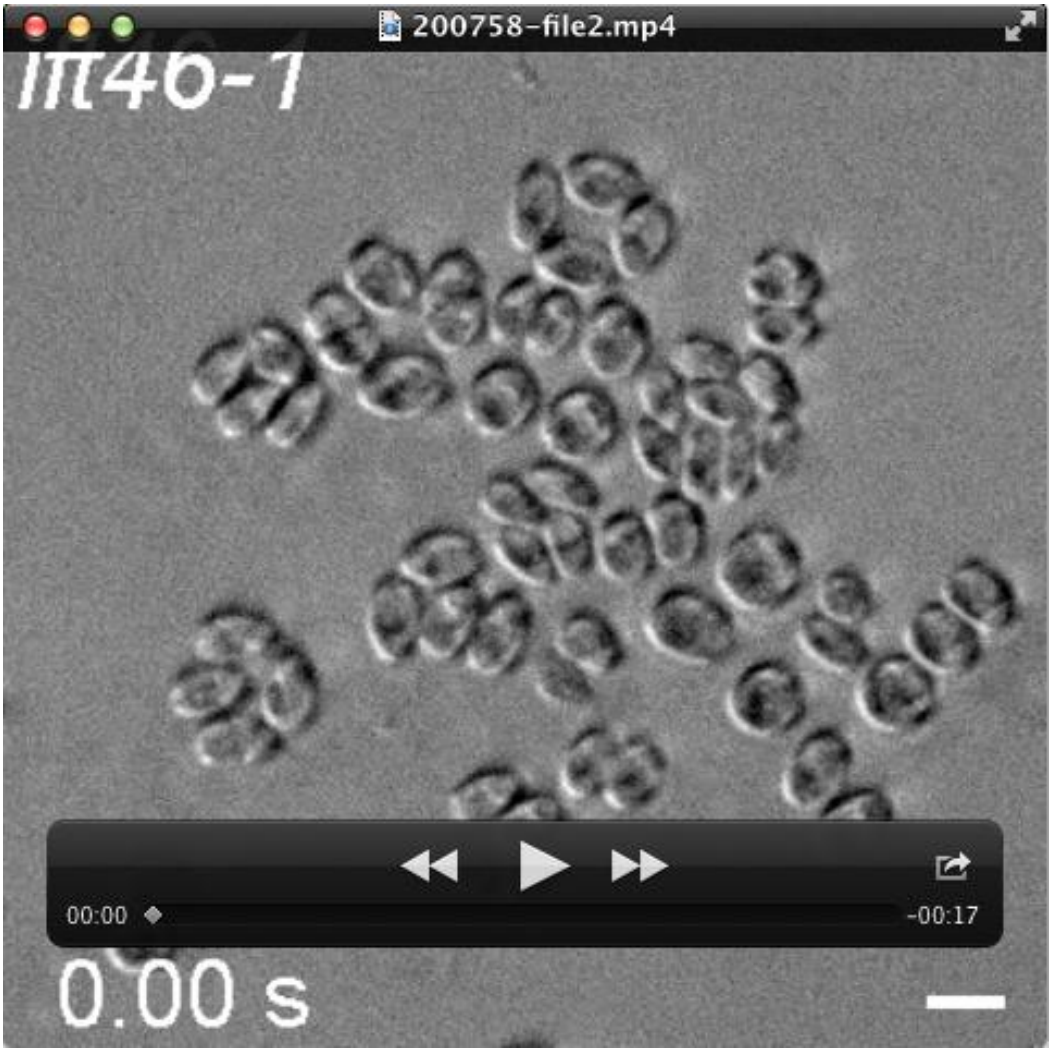

Movie 2 Immobility of *ift46-1*.

A representative movie taken for the null mutant of *IFT46*, *ift46-1*. Scale bar: 10 μm. Images were observed under a DIC microscope with a 100x objective, recorded at one frame per 0.13 sec and displayed as it is.

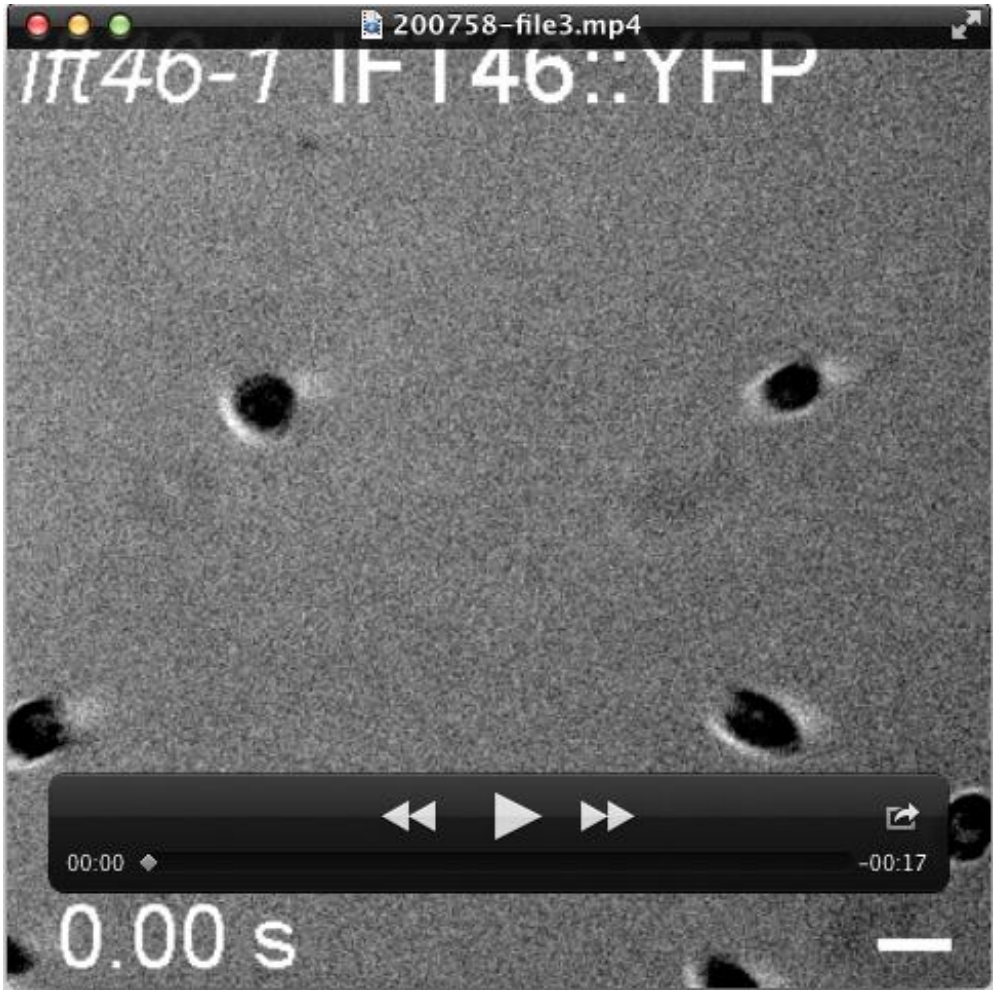

Movie 3 Locomotion of *ift46-1 IFT46::YFP*.

A representative movie taken for the rescued strain *ift46-1 IFT46::YFP*. Scale bar: 10 μm. Images were observed under a DIC microscope with a 100x objective, recorded at one frame per 0.13 sec and displayed as it is.

Movie 4 Dynamics of IFT46::YFP in the flagella of the rescued strain *ift46-1 IFT46::YFP*.

A representative movie shows IFT46::YFP in the flagella of the rescued strain *ift46-1 IFT46::YFP*. Scale bar: 10 µm. Images were observed under a total internal reflection fluorescence microscope with a 100x objective, recorded at one frame per 0.13 sec and displayed as it is.

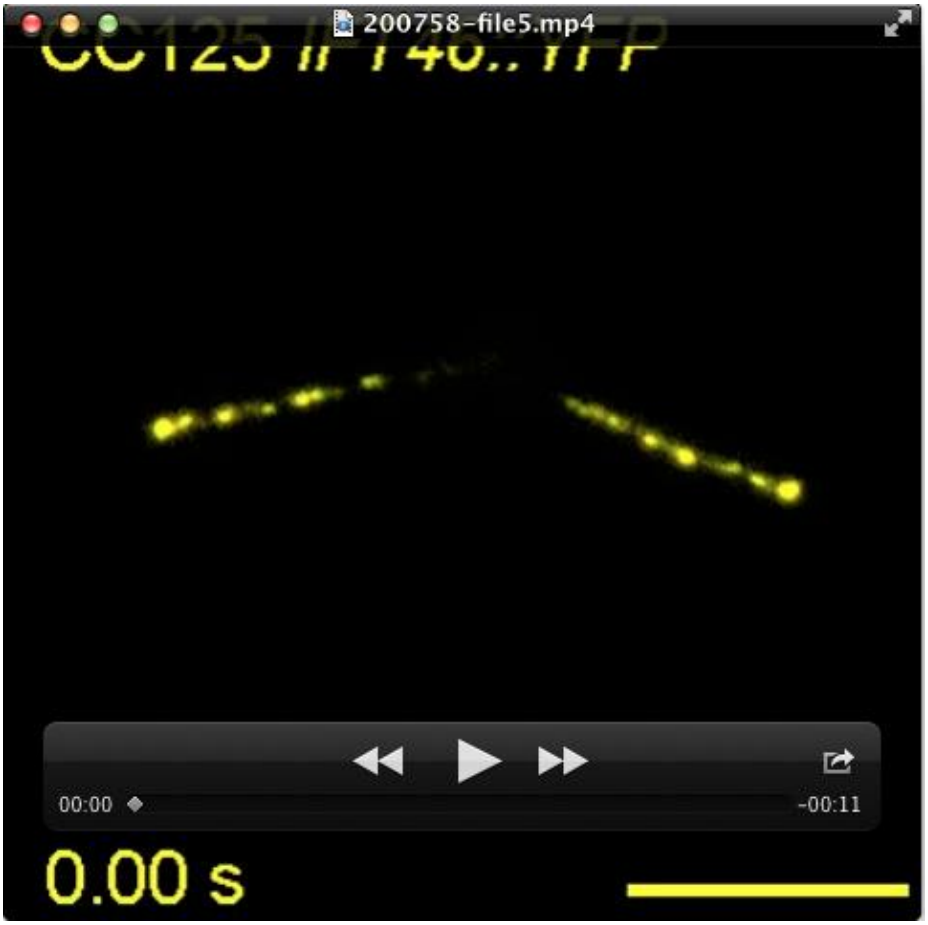

Movie 5 Dynamics of IFT46::YFP in the flagella of WT cells.

A representative movie shows IFT46::YFP in the flagella of the WT cells. Scale bar: 10 μm. Images were observed under a total internal reflection fluorescence microscope with a 100x objective, recorded at one frame per 0.13 sec and displayed as it is.

Movie 6 Dynamics of IFT46ΔN1::YFP in the flagella of WT cells.

A representative movie shows IFT46ΔN1::YFP in the flagella of the WT cells. Scale bar: 10 μm. Images were observed under a total internal reflection fluorescence microscope with a 100x objective, recorded at one frame per 0.13 sec and displayed as it is.

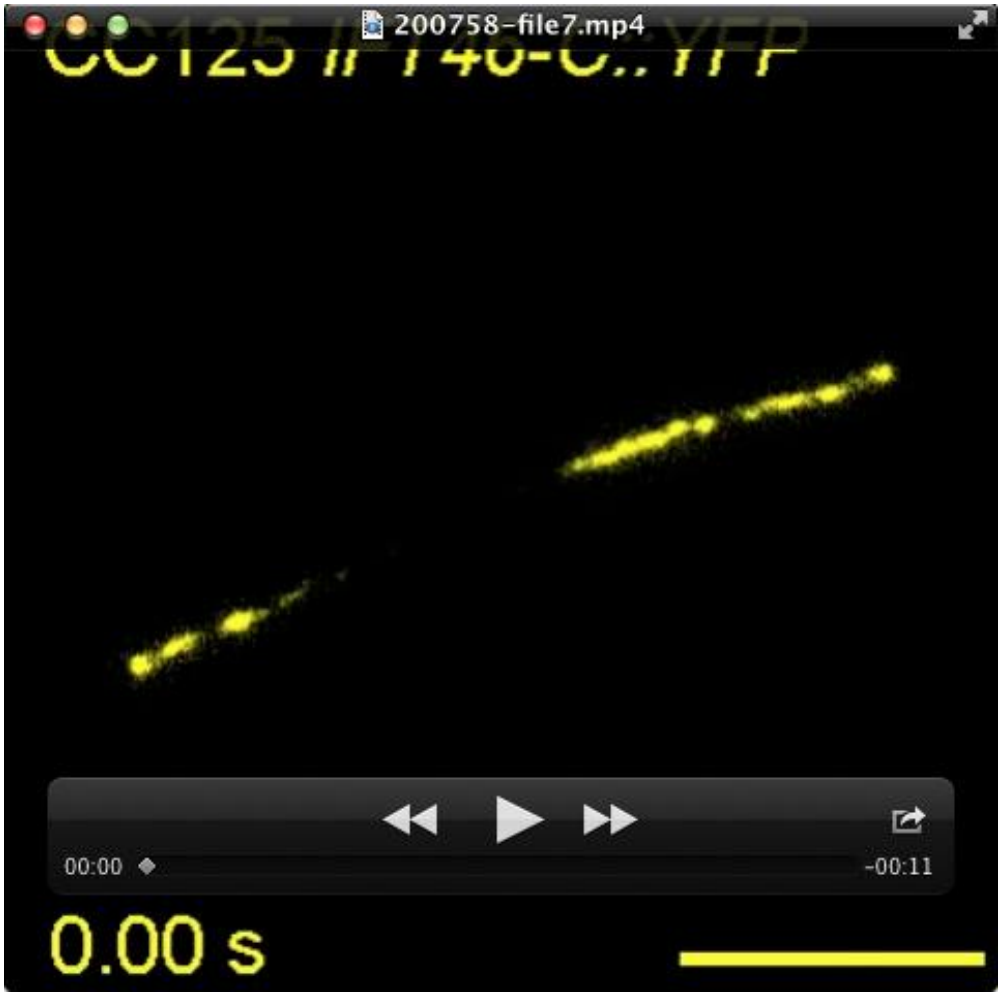

Movie 7 Dynamics of IFT46-C::YFP in the flagella of WT cells.

A representative movie shows IFT46-C::YFP in the flagella of the WT cells. Scale bar: 10 μm. Images were observed under a total internal reflection fluorescence microscope with a 100x objective, recorded at one frame per 0.13 sec and displayed as it is.

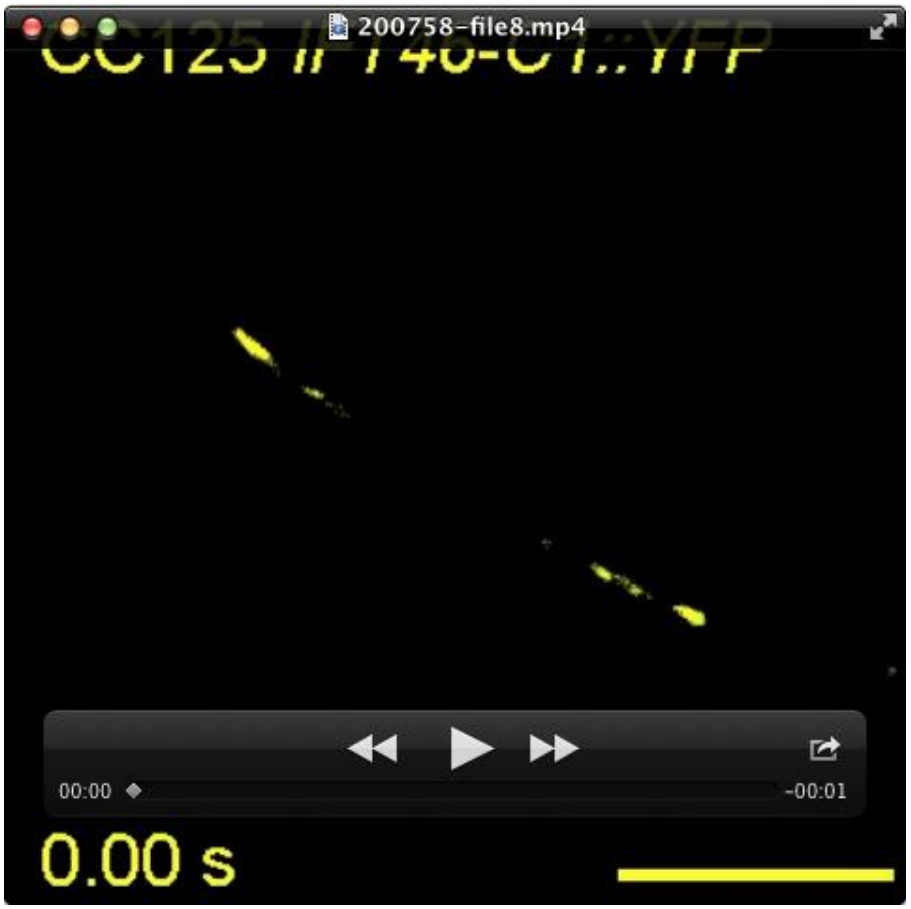

Movie 8 Dynamics of IFT46-C1::YFP in the flagella of WT cells.

A representative movie shows IFT46-C1::YFP in the flagella of the WT cells. Scale bar: 10 μm. Images were observed under a total internal reflection fluorescence microscope with a 100x objective, recorded at one frame per 0.13 sec and displayed as it is.

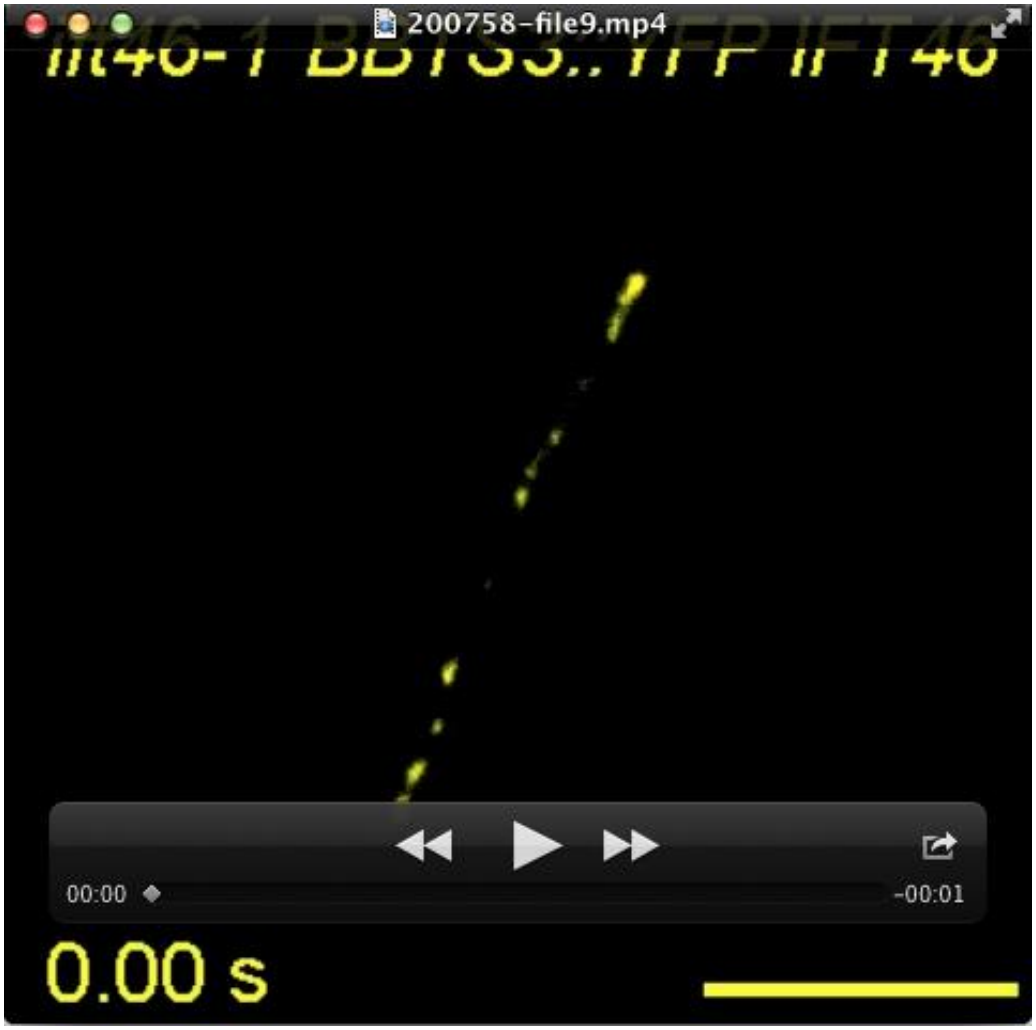

Movie 9 Dynamics of BBTS3::YFP in the flagella of strain *ift46-1 BBTS3::YFP IFT46*.

A representative movie shows BBTS3::YFP in the flagella of strain *ift46-1 BBTS3::YFP IFT46*. Scale bar: 10 µm. Images were observed under a total internal reflection fluorescence microscope with a 100x objective, recorded at one frame per 0.13 sec and displayed as it is.